PLOS COMPUTATIONAL BIOLOGY

RESEARCH ARTICLE

Impact on backpropagation of the spatial heterogeneity of sodium channel kinetics in the axon initial segment

Benjamin S. M. Barlow[1]*, **André Longtin**[1,2,3], **Béla Joós**[1,2]*

1 Department of Physics, University of Ottawa, STEM Complex, 150 Louis-Pasteur Pvt, Ottawa, Ontario, Canada, **2** Center for Neural Dynamics and AI, University of Ottawa, Ottawa, Ontario, Canada, **3** Department of Cellular and Molecular Medicine, Faculty of Medicine, University of Ottawa, Ottawa, Ontario, Canada

* BBarl039@uOttawa.ca (BSMB); BJoos@uOttawa.ca (BJ)

Citation: Barlow BSM, Longtin A, Joós B (2024) Impact on backpropagation of the spatial heterogeneity of sodium channel kinetics in the axon initial segment. PLoS Comput Biol 20(3): e1011846. https://doi.org/10.1371/journal.pcbi.1011846

Editor: Jonathan Rubin, University of Pittsburgh, UNITED STATES

Received: September 25, 2023

Accepted: January 21, 2024

Published: March 15, 2024

Data Availability Statement: Model code is available on ModelDB at https://modeldb.science/267088.

Funding: We acknowledge the support of the Natural Sciences and Engineering Research Council of Canada (NSERC), to BJ (RGPIN-2018-06835) and AL (RGPIN-2014-06204). The funders had no role in study design, data collection and analysis, decision to publish, or preparation of the manuscript.

Abstract

In a variety of neurons, action potentials (APs) initiate at the proximal axon, within a region called the axon initial segment (AIS), which has a high density of voltage-gated sodium channels (Na_Vs) on its membrane. In pyramidal neurons, the proximal AIS has been reported to exhibit a higher proportion of Na_Vs with gating properties that are "*right-shifted*" to more depolarized voltages, compared to the distal AIS. Further, recent experiments have revealed that as neurons develop, the spatial distribution of Na_V subtypes along the AIS can change substantially, suggesting that neurons tune their excitability by modifying said distribution. When neurons are stimulated axonally, computational modelling has shown that this spatial separation of gating properties in the AIS enhances the backpropagation of APs into the dendrites. In contrast, in the more natural scenario of somatic stimulation, our simulations show that the same distribution can impede backpropagation, suggesting that the choice of orthodromic versus antidromic stimulation can bias or even invert experimental findings regarding the role of Na_V subtypes in the AIS. We implemented a range of hypothetical Na_V distributions in the AIS of three multicompartmental pyramidal cell models and investigated the precise kinetic mechanisms underlying such effects, as the spatial distribution of Na_V subtypes is varied. With axonal stimulation, proximal Na_V *availability* dominates, such that concentrating *right-shifted* Na_Vs in the proximal AIS promotes backpropagation. However, with somatic stimulation, the models are insensitive to *availability* kinetics. Instead, the higher *activation* threshold of *right-shifted* Na_Vs in the AIS impedes backpropagation. Therefore, recently observed developmental changes to the spatial separation and relative proportions of $Na_V1.2$ and $Na_V1.6$ in the AIS differentially impact *activation* and *availability*. The observed effects on backpropagation, and potentially learning via its putative role in synaptic plasticity (e.g. through spike-timing-dependent plasticity), are opposite for orthodromic versus antidromic stimulation, which should inform hypotheses about the impact of the developmentally regulated subcellular localization of these Na_V subtypes.

Competing interests: The authors have declared that no competing interests exist.

Author summary

Neurons use sodium ion currents, controlled by a neuron's voltage, to trigger signals called action potentials (APs). These APs typically result from synaptic input from other neurons onto the dendrites and soma. An AP is generated at the axon initial segment (AIS) just beyond the soma. From there, it travels down the axon to other cells, but can also propagate "backwards" into the soma and dendrites. This "backpropagation" allows the neuron to compare the timing of outgoing and incoming signals at synapses where input was received, a feedback process that modifies its connections to other neurons (spike-timing-dependent synaptic plasticity) which is a mechanism for learning. It is puzzling that in many neurons, sodium ion channels come in two types: high-voltage threshold channels clustered near the soma where the AIS begins, and low-voltage ones further away towards the axon. This separation changes in the early development of the animal, which raises the question of its role in backpropagation. We constructed detailed mathematical models to explore how separation affects backpropagation. Separation either impedes or enhances backpropagation, depending on whether the AP results from input to the soma or dendrites or, less typically, input received in the axon. This is explained by the different effects the separation has on two key kinetic processes that govern sodium currents.

Introduction

In fluorescence microscopy images of neurons, the axon initial segment (AIS) is visible as a patch of axonal membrane near the soma with a high density of voltage-gated ion channels. These channels enable the AIS to initiate and shape action potentials (spikes) and regulate neuronal excitability [1]. The AIS can be thought of as an organelle that lives within the first ≈ 100μm of axonal membrane and whose function it is to supply the current needed to initiate spikes when the neuron is poised to fire—usually in response to synaptic input. The AIS can move up and down the axon and also change its length on a timescale of hours to days. This phenomenon, called structural AIS plasticity, enables neurons to optimize their sensitivity to specific input frequencies during development and to homeostatically adjust their intrinsic excitability [2–4]. GABAergic input can also impinge on the AIS from axo-axonic synapses, such that the AIS can be modulated directly by interneurons. Synaptic input at the AIS can rapidly and precisely control the excitability of individual neurons for sound localization [5]. Fast AIS plasticity, including receptor-mediated changes to local ion channel properties and endocytosis of voltage-gated channels, occurs on timescales of seconds to minutes [6]. (This is distinct from pathological remodelling induced by ischemia, although in [7], it was recently demonstrated that cortical neurons are more robust to interruptions in blood flow than previously thought.) The outsized electrophysiological influence of the AIS demands robust characterization of this short piece of axon as it interacts with its environment.

Over three-quarters of all neurons in the mammalian cortex are pyramidal cells (see Fig A in S1 Text), which have dendrites spanning the thickness of the cortex (several mm) and AIS lengths on the order of tens of μm [8–11]. The AIS requires a high density of voltage-gated sodium channels (Na_Vs) to prime and initiate action potentials (APs) [12–14]. In pyramidal cells, the AIS features two Na_V subtypes, with an interesting spatial distribution: $Na_V1.2$ channels cluster near the soma (i.e. at the proximal AIS) while $Na_V1.6$ cluster toward the distal AIS [15–17]. However, the purpose of this separated distribution of Na_V subtypes remains unclear [18, 19]. Further, recent experiments have revealed that as neurons develop, the spatial

distribution of Na_Vs in the AIS can change substantially, suggesting that neurons tune their excitability by modifying said distribution [20].

Our modelling study is motivated by the following question: What effect does the separated spatial distribution of $Na_V1.2$ and $Na_V1.6$ in the AIS have on excitability and backpropagation? And does the answer depend on whether stimulation is orthodromic or antidromic? In particular, how does the finding in [15], that the separated distribution of Na_V subtypes favours backpropagation—simulated with axonal (antidromic) current injection—generalize to the more common situation of somatic (orthodromic) stimulation?

It is a prevalent view that the Hodgkin-Huxley style kinetics of $Na_V1.2$ are *right-shifted* relative to those of $Na_V1.6$ by an amount $V_{RS} \sim 10 - 15\text{mV}$ [13–15, 17, 21, 22]. Due to their *right-shifted* gating properties (see Fig P in S1 Text), $Na_V1.2$ channels are often described as "high-threshold" channels, since the *right-shift* increases their half-*activation* voltage, relative to $Na_V1.6$. Because the same *right-shift* also increases $Na_V1.2$ *availability*—i.e. it reduces the proportion of inactivated $Na_V1.2$ channels at a given voltage, compared to $Na_V1.6$—it is an over-simplification for the purposes of this study to call them high- and low-threshold channels, respectively. For this reason we instead say that $Na_V1.2$ channels are *right-shifted*.

Interestingly, $Na_V1.6$ invades the proximal AIS as pyramidal neurons mature [20]. To be meaningful, the statement of Hu et al. that concentrating $Na_V1.2$ in the proximal AIS promotes backpropagation [15], requires that the *right-shifted gating properties* of $Na_V1.2$ do the promoting: Suppose a given stimulus is just barely sufficient to evoke a backpropagating AP (BAP) in the neuron with $Na_V1.2$ concentrated in the proximal AIS and $Na_V1.6$ in the distal AIS. If the function of said channel distribution is to ensure backpropagation of the AP to the soma and dendrites (as stated in [15]), then backpropagation should fail with the same stimulus if the proximal AIS were instead populated with $Na_V1.6$.

In [15], the rôle of $Na_V1.2$ in promoting backpropagation is contingent upon simulations wherein the density of $Na_V1.2$ was incrementally lowered in the AIS. However, at the proximal AIS, the active Na^+ conductance was almost entirely composed of $Na_V1.2$ channels. It does not follow then, that concentrating $Na_V1.2$ in the proximal AIS promotes backpropagation, from the fact that removing *the only* Na_V channels in that area (which happen to be $Na_V1.2$ at that developmental stage [20]) stopped backpropagation.

A more recent experimental paper which is the most directly relevant to [15] is Katz et al. (2018) [18], which compared AP thresholds in engineered mouse pyramidal neurons lacking $Na_V1.6$ to wild-type neurons with $Na_V1.2$ and $Na_V1.6$ in the AIS. In [18], they downplay the importance of Na_V subtypes in determining the excitability differences seen in the proximal versus distal AIS. Whereas antidromic stimulation was used in [15], orthodromic stimulation (somatic current injection) was used in [18]. There were no data available that isolated the effect of orthodromic versus antidromic stimulation w.r.t. the role of Na_V subtypes in the AIS in setting the backpropagation threshold. Here our modelling shows that the stimulation site matters, and can invert the experimental conclusions, which should motivate a comparative experimental study.

The separated Na_V distribution is reported to promote backpropagation—which is important for learning—following axonal stimulation [15]. There is also evidence that mutations which alter the gating properties of $Na_V1.2$ are involved in epilepsy and autism [23]. Backpropagated spikes drive learning by depolarizing the postsynaptic membrane, which triggers metabolic events that give rise to synaptic plasticity, including spike-timing-dependent plasticity [24]. There is experimental evidence that postsynaptic backpropagation can release retrograde messengers into the synapse, and influence the future release of neurotransmitters from the presynaptic neuron [25]. A backpropagating action potential can also underlie bursting in cortical neurons as it can return to the cell body from the dendrites as a depolarizing after-potential,

which in turn can initiate another somatic AP [26, 27]. Bursting can also occur in layer 5 pyramidal cells following the generation of a dendritic BAP-activated Ca^{2+} spike (BAC spike), e.g. in the presence of synaptic input. The associated BAPs can further influence the dendritic dynamics [28–31].

Not all layer 5 pyramidal cells can generate dendritic spikes as the size of the apical dendritic tree varies [32]. Dendritic spikes have also been reported to vary across species, and are not common in human layer 5 pyramidal cells [33], owing partly to their enhanced dendritic compartmentalization [34]. Thus, to further understand the original reports that Na_V segregation promotes BAPs, we investigate how Na_V segregation in the AIS can decrease the BAP threshold (described below) using the model of [15] (itself based on [26]). This provides the backbone to study the basic effects on BAPs of the AIS excitability profile, under both somatic and axonal stimulation. For the sake of generality, we complement these results by considering a state-of-the-art model of layer 5 pyramidal cells with perisomatic BAPs and dendritic BAC firing [29], adapted to include a more realistic AIS and axon.

Other computational powers are attributed to the AIS. Moving the initiation site away from the soma (i.e. toward the distal AIS) beyond a critical distance enables high-frequency spiking in cortical neurons, increasing the maximum spike frequency by an order of magnitude [14]. Separating $Na_V1.6$ into the distal AIS is said to push the initiation site toward that location, owing to those channels' lower voltage threshold [15, 21]. However, in [35], simulations having only one Na_V type demonstrated that passive cable properties are sufficient to locate AP initiation at the distal AIS.

In our simulations, we alter the composition of the AIS and look for changes in the backpropagation threshold. We distribute *right-shifted* Na_V gating properties along the AIS by differentially distributing two functionally distinct classes of sodium channels, referred to here as $Na_V1.2$ and $Na_V1.6$ following [15, 21] and [20]. We systematically alter the Na_V distribution, by varying the extent to which Na_V subtypes are spatially segregated in the AIS without affecting the total Na_V density.

We compute the threshold for backpropagation as the amplitude of a brief current pulse that causes an AP to propagate back into the dendrites and cause a sufficient depolarization (Sections B and C in S1 Text). This is done in three biophysically detailed and independently tuned multicompartmental pyramidal cell models ([15, 29]), two of which are based on the Hu et al. (2009) model and involve the same morphology but with differing soma-dendrite excitability balance (cell geometries are provided in Figs A and B in S1 Text). This threshold is computed as a function of the spatial segregation of the Na_V subtypes in the AIS by continuously varying their density profiles from fully overlapping to strongly separated (Fig 1).

We show that Na_V separation reduces the backpropagation threshold with axonal stimulation but can impede backpropagation with somatic stimulation. This asymmetrical result was not expected. To explain our results, we independently modify the *right-shift* (V_{RS}) of selected $Na_V1.2$ gating variables and their respective time constants by an amount ΔV_{RS} (i.e. $V_{RS} \rightarrow V_{RS} + \Delta V_{RS}$). These modifications to $Na_V1.2$ gating are applied only in the AIS.

Sweeping ΔV_{RS} (while clamping other gating variables to nominal V_{RS} values) reveals that (I) $Na_V1.2$ *availability* and its time constant explain how proximal $Na_V1.2$ promotes backpropagation with axonal stimulation, and (II) the threshold of steady-state *activation* explains how $Na_V1.2$ suppresses backpropagation and reduces excitability with somatic stimulation.

Being a feature of pyramidal cells, the plastic distribution of AIS Na_V subtypes that we model applies to something like eight out of ten cortical neurons [8]. Various experimental and computational techniques used to study the biophysical determinants of AIS excitability across the lifespan have involved different stimulation sites [36, 37]. Here we demonstrate

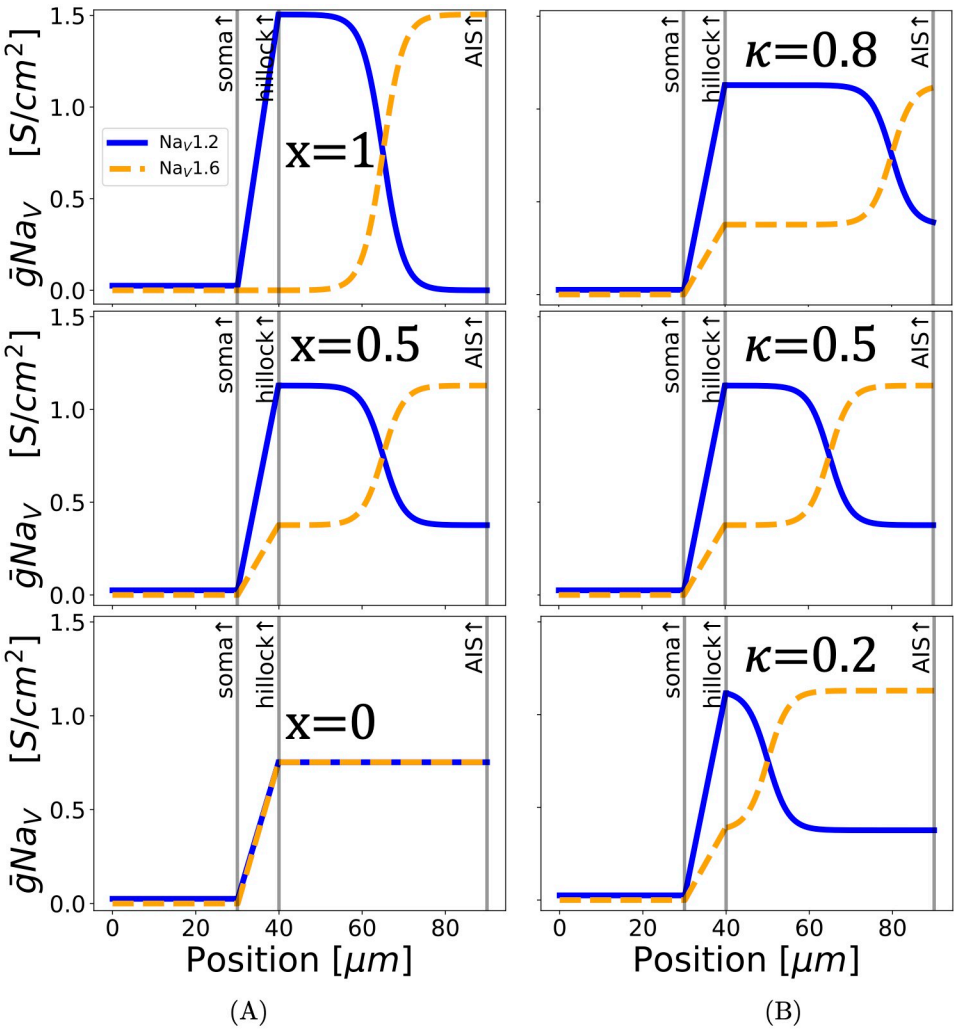

Fig 1. Modifying the spatial distribution of Na$_V$ subtypes in the AIS while keeping the total conductance constant. (**A**) The spatial separation of Na$_V$ subtypes in the AIS is varied using the parameter "x" with $\kappa = 0.5$. The top plot is a model setup with a separated distribution [15, 20] of Na$_V$s in the AIS. The high threshold Na$_V$1.2 (indicated in blue) are concentrated close to the soma, and the low threshold Na$_V$1.6 (indicated in orange) are kept distal to the soma. Moving from top to bottom, both Na$_V$ subtypes are distributed ever more evenly along the AIS. We chose the parameter name "x" to vary the spatial separation of the AIS Na$_V$ distributions, because the separated distribution is x-shaped. Setting $x = 1$ in our simulations gives the separated distribution, and $x = 0$ gives the "flat" distribution wherein both Na$_V$ subtypes are uniformly mixed. (**B**) Variation of the crossover location (κ) of Na$_V$s in the AIS with $x = 0.5$. We have lengthened the AIS to 50μm in this graphic for visual clarity.

https://doi.org/10.1371/journal.pcbi.1011846.g001

opposing effects on backpropagation with orthodromic versus antidromic stimulation by altering the separated Na$_V$ distribution. Both stimulation modes are used by experimentalists [11, 15, 18, 38], and certain pyramidal neurons are also known to receive axo-axonic input at the AIS as well as somatodendritic input [6]. It is thus important to know whether and how the spatial profile of Na$_V$ channel subtypes really enhances backpropagation in vivo, and whether moving the stimulating electrode can bias or even invert experimental findings, as our work demonstrates. Apart from explaining the dynamical mechanism behind the dependence of AP generation on AIS Na$_V$ distribution, we clearly show that the site of stimulation matters, a finding that is present robustly in different models and which merits experimental

confirmation. Changes to AIS properties and the follow-on effects on backpropagation must affect the entire cortex.

Results

Hypothetical Na_V distributions in the AIS

We begin with our implementation of the model from Hu et al. (2009) [15] (Hu-based model), using their morphology, K_V and Na_V kinetics (for details, see Materials and methods). The standard AIS length in our model is 25 μm, based on measurements from [10]. A key feature of the Na_V distribution that changes during development, is the extent to which the voltage-gated sodium channel subtypes $Na_V1.2$ and $Na_V1.6$ are localized in the proximal and distal AIS, respectively [20]. In our simulations, the relative proportion of $Na_V1.2$ versus $Na_V1.6$ at a given position along the AIS can be changed without affecting the total Na_V density at any point (Eq 6).

Fig 1 shows how the parameters x and κ control the way Na_V subtypes are spread out along the AIS. When x is at its highest value of 1, the subtypes $Na_V1.2$ and $Na_V1.6$ are spaced apart from each other, with $Na_V1.2$ concentrated in the proximal AIS and $Na_V1.6$ in the distal AIS, approximating the distribution observed in developing pyramidal neurons (see [20]). Decreasing x transforms this separated distribution into a uniform mix ($x \to 0$) where $Na_V1.2$ and $Na_V1.6$ are distributed homogeneously. This can be seen in Fig 1A.

Every distribution except the uniform Na_V mix has a location along the AIS at which the density of $Na_V1.6$ overtakes the $Na_V1.2$ density. That location, which we call the Na_V crossover and denote κ, is also varied in our simulations (see Fig 1A; κ is a dimensionless length normalized by the AIS length).

To cement our results, we will further apply identical transformations to the Na_V distribution in a cell having a 'backward' AIS, that is, with *distal* $Na_V1.2$ and *proximal* $Na_V1.6$. The results from the backward AIS model are nearly a mirror image of our findings.

For each hypothetical Na_V distribution, a short current pulse (1ms) is injected at a specific site, and the minimum (i.e. threshold) pulse amplitude I (in nA) required to elicit a spike is determined. Brief pulse durations separate the stimulation waveform from the intrinsic response of the cell. We define excitability in terms of two thresholds: backpropagation threshold I_{BP} (AP leading to a spike in the distal dendrites) and forward-propagation threshold I_{FP} (axonal AP threshold, recorded without regard to the amplitude of the somatodendritic depolarization).

Current is injected either in the middle of the soma (somatic stimulation) or the axon just distal to the AIS (axonal stimulation). In both cases, forward propagation refers to an AP travelling down the axon, and backpropagation always refers to an AP visible as a spike in the dendrites. Backpropagation was deemed to have occurred if all apical dendritic tips exceeded −63.0mV (i.e. a depolarization of 7.0mV above V_{rest}) following stimulation (see Fig C in S1 Text).

In the following sections, we implement the above Na_V distributions in the Hu-based model [15] (Fig A in S1 Text), which we chose as a starting point because of its seminal role in the study of how Na_V subtypes in the AIS affect backpropagation. At V_{rest}, the *activation* of $Na_V1.2$ and $Na_V1.6$ is negligible, so the total conductance at rest is not affected by x or κ (see Fig Pi in S1 Text).

Due to the "curse of dimensionality" and limitations in the spatial resolution of experimental measurements, many parameters in multicompartmental models—such as the density of ion channels at every point on the cell membrane—must be estimated and require tuning, introducing subjective judgement on the part of the modeller (reviewed in [39]). Hu et al. [15]

based their simulations on a hand-tuned model from [26]. The adjustment and re-adjustment of hand-tuned models is a potentially endless cycle [39]. It is desirable to have a model which is tuned automatically via an objective procedure, to break the loop of hand-tuning. To this end, in Generalization to Hay-based model and modified Hu-based model, we repeat the procedure described above—i.e. varying the Na_V distributions in the AIS as in Fig 1—in the model of Hay et al. (2011) [29] (Fig B in S1 Text). Hay et al. used an evolutionary algorithm to optimize the densities of nine simulated ion channels in each compartment of reconstructed layer-5b pyramidal neurons. The ground truth in that fitting consisted of somatodendritic spiking patterns recorded in a variety of such neurons from adult rats.

The third model, a modification of our Hu-based model with significant qualitative differences in its backpropagating action potential, is included in Section D in S1 Text. In the latter model, the dendritic excitability is much higher, with negligible attenuation of the backpropagating action potential. The dendritic Na_V density is increased 10-fold relative to the Hu-based model in the main text, and the somatic Na_V density is decreased 3-fold. Multiple models with differing conductances, biophysics, and morphology demonstrate the robustness of our results, as we can modify the density profiles of $Na_V1.2$ and $Na_V1.6$ in the AIS without affecting any other compartments. For further details, see Materials and methods and S1 Text.

Somatic stimulation

In Fig 2, both negatively and positively sloped backpropagation threshold curves with respect to x are present, indicating that Na_V separation can promote or impede backpropagation (respectively). Changes in threshold can be as large as 30%. Moving the Na_V crossover (κ) toward the distal AIS shifts the backpropagation threshold curves upward. A qualitative change, namely the sign of the slope, occurs around $\kappa = 0.4$.

An intuitive explanation for this latter effect is that moving the crossover location away from the soma causes the AIS to be dominated by $Na_V1.2$ channels (see Fig 1B, $\kappa = 0.8$), which have a higher *activation* voltage threshold than $Na_V1.6$. APs still initiate in the distal AIS, but the dominant $Na_V1.2$ renders the cell less excitable. Further, for $\kappa \gtrsim 0.4$, the backpropagation threshold increases as we tend toward the separated, x-shaped distribution of Na_Vs. This behaviour is the opposite of what is observed for axonal stimulation below and in [15]. We repeated these simulations with AIS length up to 100μm (Fig L in S1 Text) and also with stimulation at the main apical dendrite (Fig N in S1 Text) instead of the soma, and obtained the same qualitative results as Fig 2 (see Section D.1 in S1 Text).

The negatively sloped curves do not necessarily imply that proximal $Na_V1.2$ promotes backpropagation in the case of somatic stimulation. In those curves ($\kappa \lesssim 0.4$), the AIS is mainly populated with $Na_V1.6$ when $x > 0$. Also note that decreasing κ places more $Na_V1.6$ channels nearer to the soma (see Fig 1B, $\kappa = 0.2$). In that case, the threshold-lowering effect of Na_V separation could come from the increased total $Na_V1.6$ density that results from increasing x when κ is relatively small, rather than from the proximal accumulation of $Na_V1.2$ with increasing x. Further, increasing κ (which increases the ratio of $Na_V1.2$ to $Na_V1.6$ in the AIS) raises the threshold for all curves in Fig 2 (see also Fig M in S1 Text). It is then consistent to postulate that for somatic stimulation, the backpropagation threshold is increased by AIS $Na_V1.2$ at all values of x and κ, and Fig 2 is consistent with AIS $Na_V1.6$ enhancing excitability and backpropagation. In other words, for **somatic stimulation**:

- when $\kappa < 0.5$ and $x > 0$, the AIS is dominated by $Na_V1.6$: increasing x decreases the proportion of total AIS Na_V conductance due to $Na_V1.2$ (negative slope: separated distribution yields the lowest backpropagation threshold).

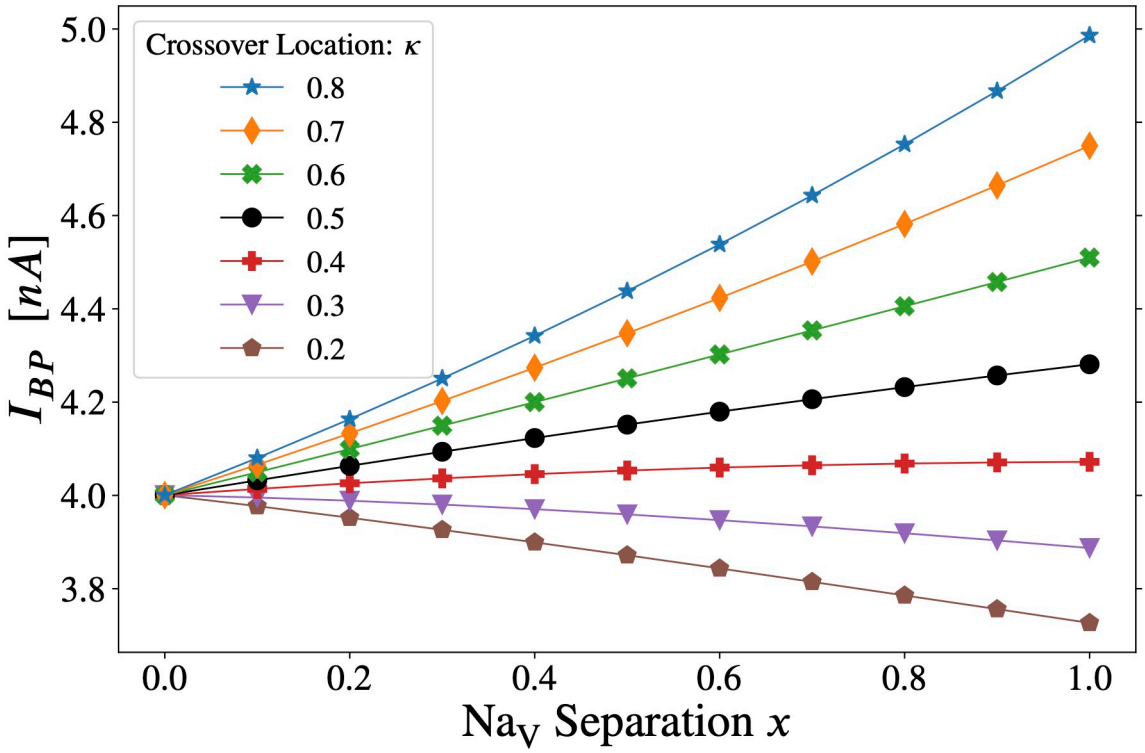

Fig 2. Somatic stimulation: Combined effect of varying crossover location (κ) and Na_V separation (x) in the axon initial segment. The threshold for forward AP propagation is the same as for backpropagation. Varying the separation parameter "x" from $x = 0$ to $x = 1$, the distribution of Na_V channels goes from flat (homogeneous) to separated, the latter approximating the distribution observed in developing pyramidal neurons (see Fig 1A). Note that curves for all values of κ converge to a single point at $x = 0$, since κ can have no effect when the two Na_V subtypes are uniformly distributed along the AIS. The lines have been drawn to guide the eye.

https://doi.org/10.1371/journal.pcbi.1011846.g002

- when $\kappa > 0.5$ and $x > 0$, the AIS is dominated by $Na_V1.2$: increasing x increases the proportion of total AIS Na_V conductance due to $Na_V1.2$ (positive slope: separated distribution yields the highest backpropagation threshold).

This effect is shown in Fig R in S1 Text. Although the above description is an appealing simplification, the impact of the spatial separation of Na_V subtypes (x) remains important, even when the AIS has equal amounts of $Na_V1.2$ and $Na_V1.6$. In other words, the combined effect of x and κ cannot be reduced to the resulting ratio of total $Na_V1.2$ versus $Na_V1.6$.

Lengthening the hillock with κ fixed also moves the crossover away from the soma. Curves with negative slope in Fig 2 became positively sloped when the hillock was lengthened from 10μm to 30μm (Fig O in S1 Text). The forward propagation threshold for somatic stimulation with a single 1ms current pulse is not included in a separate figure since it is identical to the backpropagation threshold in this model. This does not depend on the somatic injection site. The effect of Na_V gating properties in the AIS on backpropagation threshold is examined systematically in Modifying the *right-shift* of $Na_V1.2$ gating properties in the AIS.

An informative variation on Fig 2 is shown in Fig 3C in which the AIS is "put on backward", such that $Na_V1.2$ is concentrated in the distal AIS and $Na_V1.6$ is proximal to the soma. As one might expect, the effect of varying x and κ in Fig 3 is opposite to what is seen in Fig 2, albeit with some new curvature at low κ. This reinforces the observation that proximal $Na_V1.6$ facilitates backpropagation with somatic stimulation.

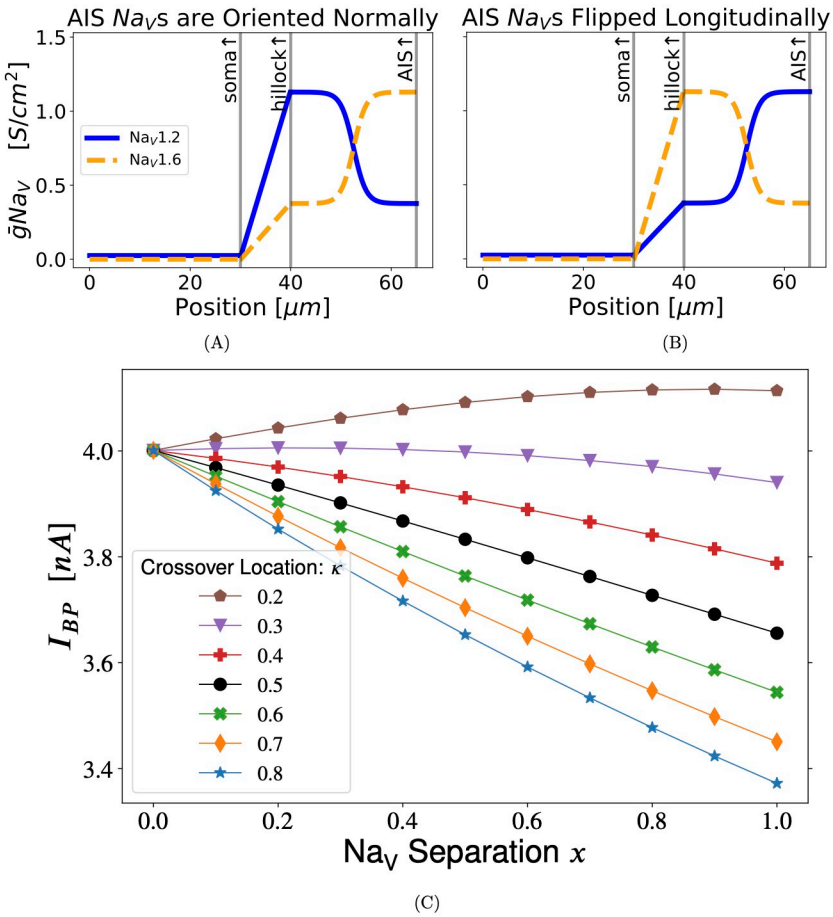

Fig 3. Somatic stimulation with a flipped Na_V distribution: Backward AIS. When the AIS Na_V distribution is flipped proximal-to-distal, setting $x = 1$ concentrates $Na_V1.6$ at the proximal AIS and $Na_V1.2$ at the distal AIS—the opposite of what is observed in many pyramidal cells [15–17]. **(A)** AIS with proper longitudinal placement of Na_Vs. **(B)** AIS with a longitudinally flipped Na_V distribution. In both plots, $x = 0.5$ and $\kappa = 0.5$. **(C)** Somatic stimulation with AIS Na_Vs flipped as in **(B)**: This result is close to a mirror image of Fig 2. The lines have been drawn to guide the eye.

https://doi.org/10.1371/journal.pcbi.1011846.g003

Axonal stimulation

With axonal stimulation (current injection just distal to the AIS), Na_V separation consistently lowers the backpropagation threshold (Fig 4). Contrary to somatic stimulation (Fig 2), moving the Na_V crossover (κ) toward the distal AIS shifts the backpropagation threshold curves downward.

The decreasing threshold with respect to x in Fig 4 is consistent with the conclusion from [15], which used axonal stimulation, that proximal $Na_V1.2$ in the AIS promotes backpropagation. Our results for κ, with axonal stimulation, provide new support for their findings.

This agreement is interesting because our method of modifying the AIS Na_V distribution (described above in Fig 1) is quite different from their simulations. Our transformations deliberately preserve the total Na_V density at every AIS segment—if $Na_V1.2$ is removed, $Na_V1.6$ must take its place. Conversely, in [15], the density profile of $Na_V1.2$ is scaled by a constant factor everywhere in the AIS, leaving the $Na_V1.6$ profile intact. We denote the scaling factor

$$\alpha_{Na_V1.2} \geqslant 0. \quad (1)$$

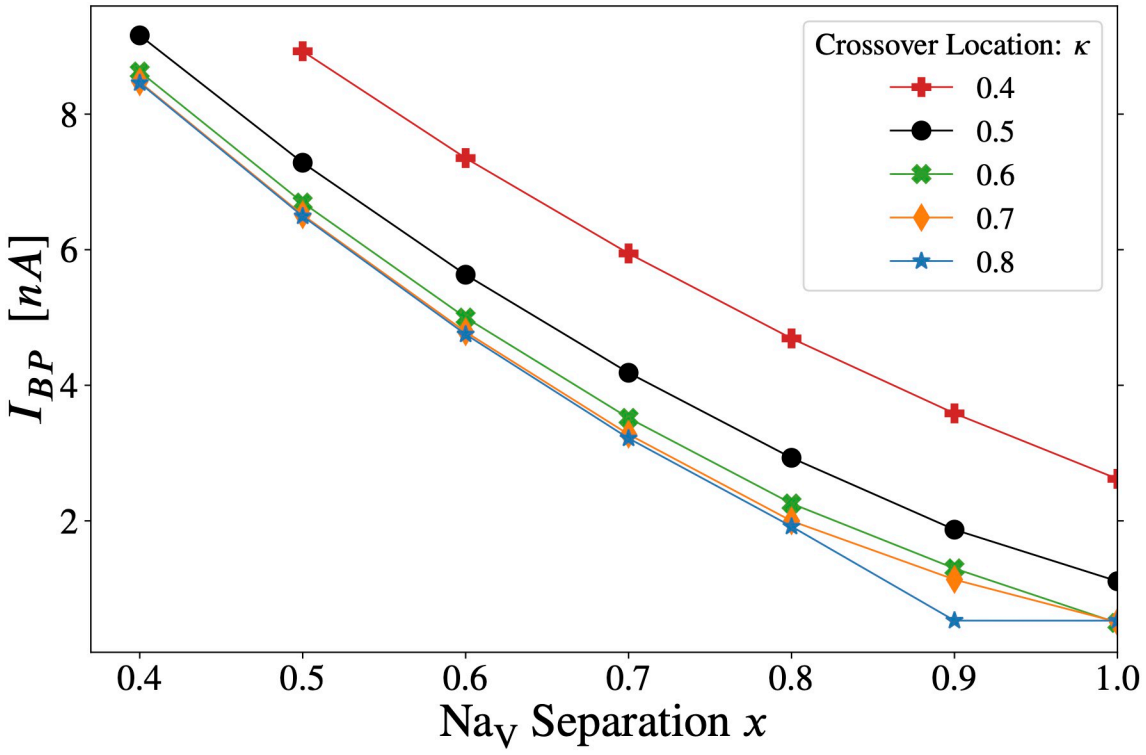

Fig 4. Axonal stimulation: Effect of varying crossover location (κ) and Na_V separation (x) in the AIS on the backpropagation threshold (see Fig 1). When computing the threshold, the stimulating current was limited to a maximum of 10nA, to prevent unphysiological local depolarization at the stimulation site. Due to the smaller diameter of the axon (relative to the soma), 10nA is sufficient to depolarize the membrane potential to $\approx +80$mV at the stimulation site, whereas the resting potential is $V_{rest} = -70$mV. To achieve backpropagation within that constraint (following axonal stimulation), our model required some amount of proximal $Na_V1.2$, delivered through the combined effects of Na_V separation ($x \gtrsim 0.5$) and a sufficiently distal crossover position $\kappa \gtrsim 0.4$. Separating the two Na_V subtypes ($x \to 1$) lowers the threshold, in agreement with the finding in [15] that proximal accumulation of $Na_V1.2$ promotes backpropagation, albeit due to different gating properties (Fig 6B). Increasing κ raises the proportion of $Na_V1.2$ (relative to $Na_V1.6$) in the AIS and lowers the backpropagation threshold as well. Threshold changes here are larger than for somatic stimulation (Fig 2). The lines have been drawn to guide the eye.

https://doi.org/10.1371/journal.pcbi.1011846.g004

That is, if the $Na_V1.2$ density profile is scaled down in [15], nothing is added to compensate for the missing channels. Under the latter transformation, we expect that $\alpha_{Na_V1.2} > 1$ would lower I_{BP} and $\alpha_{Na_V1.2} < 1$ would raise I_{BP} in our models as well, since scaling the density profile of $Na_V1.2$ in a separated distribution with a specified κ and $x > 0$ would scale the total AIS Na_V conductance, especially at the proximal AIS. We have reproduced this procedure in the Hay model, see Rescaling the $Na_V1.2$ density profile by a uniform factor in the AIS.

It is one thing to say that reducing (increasing) the total density of voltage-gated sodium channels in the proximal AIS, which happen to be $Na_V1.2$ channels, will raise (lower) the backpropagation threshold (respectively). But since we preserved the local Na_V density in our results (above), the changes to I_{BP} can only be a manifestation of the spatial heterogeneity of sodium channel *gating properties*. Since *right-shift* is the most important feature distinguishing $Na_V1.2$ from $Na_V1.6$ in this model, we included a sensitivity analysis, see Modifying the *right-shift* of $Na_V1.2$ gating properties in the AIS. The analysis in that section explains how the proximal accumulation of $Na_V1.2$ is able to simultaneously lower I_{BP} with axonal stimulation (Fig 4) and raise I_{BP} with somatic stimulation (Fig 2).

Forward propagation threshold

The forward-propagation threshold I_{FP}, also referred to as the AP threshold, is shown in Fig 5 for the Hu-based model. With axonal stimulation only, it is possible to elicit an action potential without creating sufficient depolarization in the apical dendrites to meet our strict criterion for backpropagation (see Figs D and C in S1 Text). Note, however, that the most distal dendrites depolarize to several mV above their local resting potential (see Fig Dii in S1 Text). Stimulation amplitude is an order of magnitude lower than in the case of I_{BP}. This is expected with axonal stimulation due to the high Na_V density of the distal AIS, its electrical isolation from the soma, its proximity to the stimulus, and our stringent definition of I_{BP} (Section B in S1 Text). (Antidromically stimulated axonal APs that do not trigger a somatodendritic BAP have been observed in several neuron types [36, 37].) Further, as discussed in [39], Hu et al. [15] built their model on [26], in which somatic invasion of the axonal action potential is reduced.

As with I_{BP}, increasing x lowers I_{FP}. Na_V separation concentrates $Na_V1.6$ in the distal AIS, making it more excitable in the portion nearer to the stimulation site. This finding is consistent with [15], who found that distal $Na_V1.6$ density places the lowest initiation threshold (and therefore the AP trigger zone) at the distal AIS. However, [35] has shown that cable properties are sufficient to explain why the trigger zone is located at the distal AIS (see Discussion). Moving the crossover distally ($\kappa \to 1$) increases the total proportion of $Na_V1.2$ in the AIS and thereby raises the I_{FP} threshold due to *activation right-shift*.

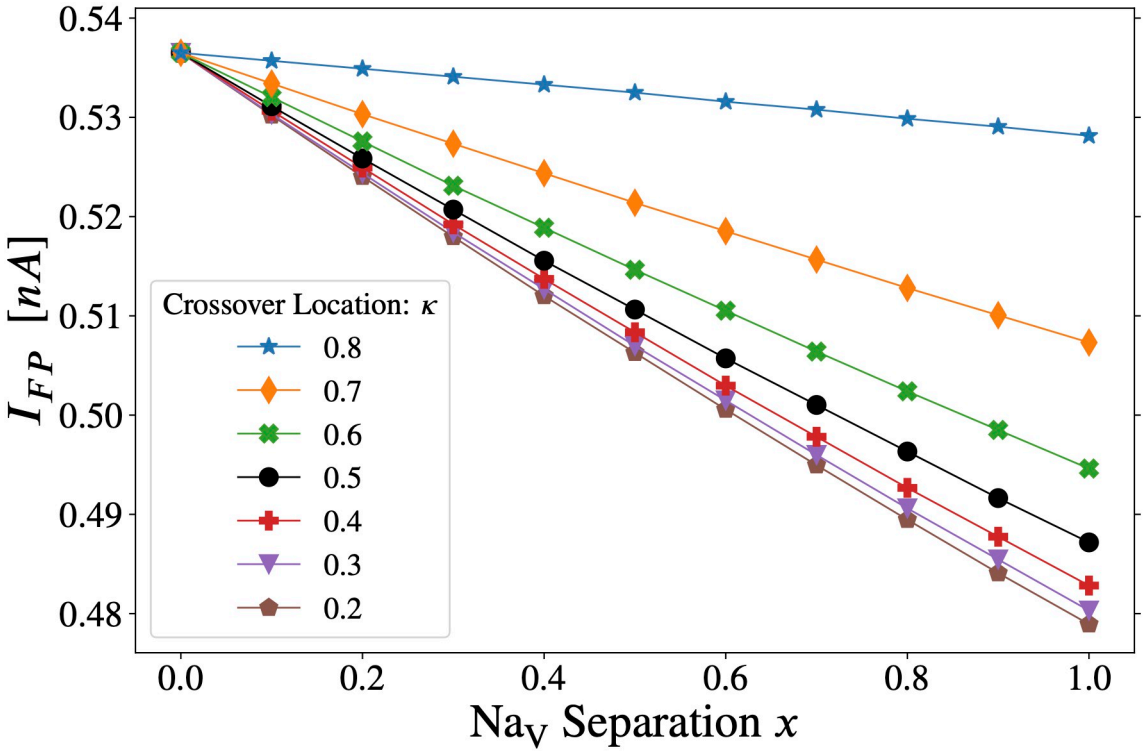

Fig 5. Axonal stimulation: Effect of x and κ on forward propagation threshold. The trend for all constant κ curves is that raising the proportion of total AIS $Na_V1.6$ (by reducing κ) or concentrating $Na_V1.6$ in the distal AIS (by increasing x) lowers the threshold to initiate forward propagating action potentials (see Fig 1). Note that although this threshold current pulse is not sufficient to satisfy our strict backpropagation criterion (see Section B in S1 Text), the most distal apical dendrites will be depolarized by several mV relative to their local resting potential (see Fig Dii in S1 Text). The lines have been drawn to guide the eye.

https://doi.org/10.1371/journal.pcbi.1011846.g005

Modifying the *right-shift* of $Na_V1.2$ gating properties in the AIS

Our results from varying the Na_V distribution may be counterintuitive. With axonal stimulation, concentrating low-threshold (i.e. *left-shifted*) $Na_V1.6$ channels at the distal AIS ought to promote forward propagation (and it does, see Fig 5), but why would concentrating the high-threshold (i.e. *right-shifted*) $Na_V1.2$ channels at the proximal AIS promote [15] backpropagation (see Fig 4)? And how does the asymmetry come about, such that separating Na_V subtypes can raise the backpropagation threshold with somatic stimulation, but always lowers it with axonal stimulation?

In this section, we perform a type of sensitivity analysis with respect to the effects of the *right-shifted* $Na_V1.2$ subtype. Fig 6 allows us to isolate the effects of *activation right-shift* versus *availability right-shift* on the backpropagation threshold.

Na_V subtypes are defined by their gating properties. Each Na_V distribution (Fig 1) produces a corresponding spatial profile of gating properties, including a profile of *right-shift*. (Gating properties are detailed in Section F in S1 Text, see Fig P in S1 Text.) In Fig 6, the AIS Na_Vs' separation is fixed at $x = 1$. This spatial separation of Na_Vs concentrates *right-shift* in the proximal AIS, by concentrating $Na_V1.2$ in that region (see Fig 1).

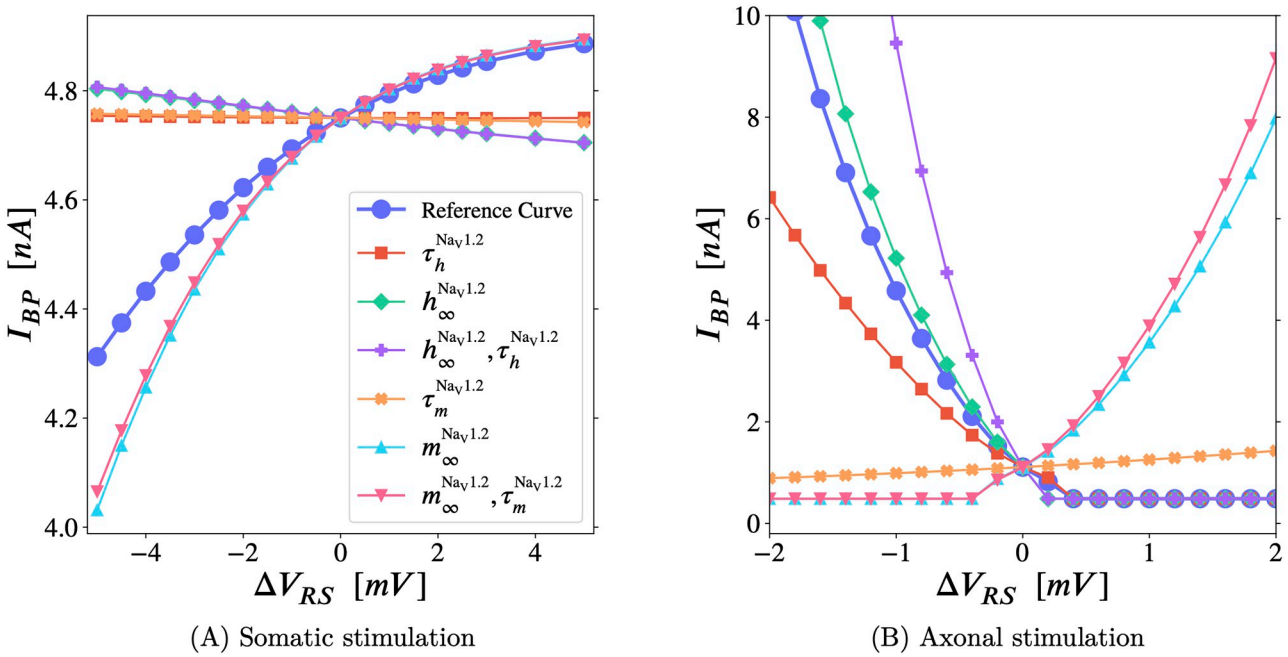

Fig 6. Sensitivity analysis of the backpropagation threshold to the *right-shift* of $Na_V1.2$ gating properties. Along each curve, the gating properties named in the legend have their *right-shift* changed from V_{RS} to $(V_{RS} + \Delta V_{RS})$, and all the others are left unchanged (full definition and notation in Section F.2 in S1 Text). When $\Delta V_{RS} = 0$, the *right-shift* is the reference value (or 'nominal value') of 13.0mV used for $Na_V1.2$ in our simulations—see Section F.2 in S1 Text, V_{RS} indicated by small "→" in Fig P in S1 Text—around which we are performing this sensitivity analysis. The reference curve (legended ●) shows the net effect of *right-shifting* all $Na_V1.2$ properties on I_{BP}, via its slope. (It may be useful to imagine points on the reference curve as being pulled toward all the other curves that only change one property. The reference curve would then be the result of the combined pulls of those curves.) For each mode of stimulation, we identify the key gating properties through which *right-shift* controls backpropagation, by comparing the single property curves (▲$m_\infty^{Na_V1.2}$, ×$\tau_m^{Na_V1.2}$, etc.) to the reference curve (●). **(A) Somatic stimulation**: The reference curve has a positive slope (*right-shift* raises I_{BP}), and it follows curves legended with $m_\infty^{Na_V1.2}$ near the nominal point (i.e. near $\Delta V_{RS} = 0$). Hence, I_{BP} is governed by Na_V steady-state *activation* and is insensitive to the *right-shift* of all Na_V time constants. **(B) Axonal stimulation**: The reference curve has a negative slope (*right-shift* lowers I_{BP}, i.e. promotes backpropagation), and it follows curves legended with $h_\infty^{Na_V1.2}$ or $\tau_h^{Na_V1.2}$. I_{BP} is then governed by proximal Na_V *availability*, owing to the *right-shift* of $Na_V1.2$. Notably, with axonal stimulation, I_{BP} is also sensitive to the *right-shift* of $\tau_h^{Na_V1.2}(V)$, the—voltage-sensitive—*availability* time constant. Results are summarized in Table 1. The lines have been drawn to guide the eye. In both plots, $x = 1.0$. On the left $\kappa = 0.7$(to increase the slope, see Fig 2), and on the right, $\kappa = 0.5$.

https://doi.org/10.1371/journal.pcbi.1011846.g006

Modifying the *right-shift* of all gating properties of $Na_V1.2$ in the AIS. Our model sets the nominal *right-shift* of $Na_V1.2$ at $V_{RS} = 13.0\text{mV}$ for compatibility with [15]. We use the parameter ΔV_{RS} to alter, in the AIS only, the *right-shift* of specific $Na_V1.2$ gating properties. (For additional details, see Sections F.2 and F.3 in S1 Text.)

When a gating property (e.g. $m_\infty^{Na_V1.2}$) appears next to a curve in the legend of Fig 6, the voltage-dependence of said property is displaced by ΔV_{RS} (see, e.g., Eq 3). Likewise, if a gating property is *not* displayed in the legend, its voltage-dependence *isn't* affected by ΔV_{RS}.

For conceptual clarity, we call the variable h—which models the process by which Na_V channels are inactivated (or blocked) in Hodgkin-Huxley style kinetics [40]—the *availability*. For example, since the $Na_V1.2$ conductance is given by $g_{Na_V1.2}(V,t) = \bar{g}_{Na_V1.2} * (m^{Na_V1.2})^3 h^{Na_V1.2}$—where $\bar{g}_{Na_V1.2}$ is the maximal conductance and $m^{Na_V1.2}$ is the *activation*—$h^{Na_V1.2}$ is the proportion of those channels which are *not* inactivated. That is, $h^{Na_V1.2}(V,t)$ is the probability that a $Na_V1.2$ channel selected at random is *available* to conduct sodium current. The inactivation is actually given by $(1 - h)$ since, in such models, all channels are inactivated when $h = 0$ and all are available when $h = 1$.

Note that the *activation* $m^{Na_V1.2}(V,t)$ and *availability* $h^{Na_V1.2}(V,t)$ of real $Na_V1.2$ channels are *right-shifted* by similar amounts when compared to the corresponding gating properties of $Na_V1.6$ [13, 15, 17, 21, 22]. (Although certain receptors can temporarily *right-shift activation* without shifting steady-state *availability* [41].) In our simulations, we can simultaneously decrease (or increase) the *right-shift* of $m^{Na_V1.2}$ and $h^{Na_V1.2}$ together, making the $Na_V1.2$ channels more (or less) similar to the $Na_V1.6$ channels in the AIS (respectively). This produces the 'reference curves' legended '●' in Fig 6A and 6B. In those curves, ΔV_{RS} shifts the voltage-dependence of every $Na_V1.2$ gating property.

That is, as functions of membrane potential, the steady states and time constants in the curves marked '●' are defined

$$\bullet \leftarrow \begin{cases} m_\infty^{Na_V1.2} = m_\infty^{Na_V1.2}(V - \Delta V_{RS}), \\ \tau_m^{Na_V1.2} = \tau_m^{Na_V1.2}(V - \Delta V_{RS}), \\ h_\infty^{Na_V1.2} = h_\infty^{Na_V1.2}(V - \Delta V_{RS}), \\ \tau_h^{Na_V1.2} = \tau_h^{Na_V1.2}(V - \Delta V_{RS}), \end{cases} \tag{2}$$

in the AIS.

Fig 6 connects local gating properties in the AIS, and their influence on the backpropagation threshold under somatic and axonal stimulation, to the effects of altering the Na_V distribution (seen above in Figs 2 and 4, respectively). For example, making ΔV_{RS} negative will *left-shift* the voltage-gated sodium current in the proximal AIS, which is analogous to adding more proximal $Na_V1.6$. However, this is merely an analogy: With $x = 1$ and $\kappa \gtrsim 0.8$, the proximal AIS has only $Na_V1.2$ channels, and positive values of ΔV_{RS} will *right-shift* the sodium current in that area beyond what is attainable by changing the local mix of Na_V subtypes.

The reference curve (●) in Fig 6A shows that *right-shifting* Na_Vs in the AIS *increases* I_{BP} for somatic stimulation. And the reference curve in Fig 6B confirms that proximal *right-shift* from $Na_V1.2$ *lowers* I_{BP} for axonal stimulation.

Modifying the *right-shift* of selected gating properties of $Na_V1.2$ in the AIS. Since ΔV_{RS} only affects $Na_V1.2$ channels *within the AIS* (example provided in Fig Qii in S1 Text), we can determine which *right-shifted* gating properties drive the changes to I_{BP} that occur when the Na_V distribution is altered. To make said observation, in Fig 6 we also "shift-clamp" selected gating properties: We ignore the experimental fact that Na_V *activation* and *availability* tend to *right-shift* in unison [17, 21, 22, 42, 43], and that the steady-state of a gating variable and its

voltage-sensitive time constant *right-shift* together as well [40]. Rather, we isolate the effects of individual $Na_V1.2$ gating properties in our simulations by shifting some of them while leaving others alone.

We can apply ΔV_{RS} to $Na_V1.2$ *availability* $h^{Na_V1.2}(V,t)$ without affecting the voltage dependence of the same channels' *activation* $m^{Na_V1.2}(V,t)$ in our model. This is done via the steady-state *availability* $h_\infty^{Na_V1.2}(V-\Delta V_{RS})$ and its voltage-dependent time constant $\tau_h^{Na_V1.2}(V-\Delta V_{RS})$, while leaving the corresponding *activation* variables—$m_\infty^{Na_V1.2}(V)$ and $\tau_m^{Na_V1.2}(V)$—unchanged. The curve legended "✚$h_\infty^{Na_V1.2}$, $\tau_h^{Na_V1.2}$" does just that, and likewise, in the "▼$m_\infty^{Na_V1.2}$, $\tau_m^{Na_V1.2}$" curve, the $Na_V1.2$ *activation* is shifted by ΔV_{RS} without affecting *availability*.

Further, we apply ΔV_{RS} to $\tau_h^{Na_V1.2}(V)$ without modifying any other gating properties—including $h_\infty^{Na_V1.2}(V)$—in the curve legended "■$\tau_h^{Na_V1.2}$". We do the same for $h_\infty^{Na_V1.2}(V)$, $\tau_m^{Na_V1.2}(V)$ and $m_\infty^{Na_V1.2}(V)$, in the curves legended "◆$h_\infty^{Na_V1.2}$", "✕$\tau_m^{Na_V1.2}$", and "▲$m_\infty^{Na_V1.2}$" respectively. Fig 6 computes the new backpropagation threshold $I_{BP}(\Delta V_{RS})$ under the aforementioned transformations. (For mathematical details, see Shift-Clamping and the Hodgkin-Huxley model in Materials and methods, and Section F.2 in S1 Text.)

An example transformation is given below by Eq 3, in which only $\tau_h^{Na_V1.2}(V)$ has its *right-shift* modified by ΔV_{RS} (see Fig Qii in S1 Text). The other three $Na_V1.2$ variables have the nominal *right-shift* of 13mV. The $I_{BP}(\Delta V_{RS})$ curves in Fig 6 that correspond to Eq 3 are legended ■$\tau_h^{Na_V1.2}$:

$$\blacksquare\tau_h^{Na_V1.2} \leftarrow \begin{cases} \tau_h^{Na_V1.2} = \tau_h^{Na_V1.2}(V-\Delta V_{RS}) \\ h_\infty^{Na_V1.2} = h_\infty^{Na_V1.2}(V) \\ \tau_m^{Na_V1.2} = \tau_m^{Na_V1.2}(V) \\ m_\infty^{Na_V1.2} = m_\infty^{Na_V1.2}(V). \end{cases} \tag{3}$$

(Fig Q in S1 Text visualizes the impact of Eq 3 on gating properties as a function of position at V_{rest}.)

To unpack these additional curves, we begin at the coordinate we will call 'the nominal point' in each plot of Fig 6, which is the backpropagation threshold at $\Delta V_{RS} = 0$, where all curves must intersect by definition. Starting at the nominal point, as one moves leftward along a given curve ($\Delta V_{RS} < 0$), the gating properties indicated in the legend are *left-shifted* (e.g. Eq 3), and the other gating properties are left alone. Likewise, travelling away from the nominal point to the right ($\Delta V_{RS} > 0$) will *right-shift* the indicated properties, relative to their nominal kinetics (Fig P in S1 Text).

Fig 6B reveals that, with axonal stimulation, the *right-shifted availability* ($h^{Na_V1.2}$) drives I_{BP}. Specifically, the curves legended ◆$h_\infty^{Na_V1.2}$, ■$\tau_h^{Na_V1.2}$, and ✚$h_\infty^{Na_V1.2}$, $\tau_h^{Na_V1.2}$ show how $h_\infty^{Na_V1.2}$ (the *availability* at steady-state, as a function of membrane potential) and $\tau_h^{Na_V1.2}$ (the voltage-dependent time constant of *availability*) work together to promote backpropagation: They drive the reference curve (●) downward as ΔV_{RS} increases, in spite of the higher *activation* threshold. In other words: The threshold-lowering effects that result from *right-shifting* the *availability* overpower the opposing influence of *right-shifted activation*—on its own the latter would raise the threshold (see the curves: ▲$m_\infty^{Na_V1.2}$ and ▼$m_\infty^{Na_V1.2}$, $\tau_m^{Na_V1.2}$ in Fig 6B).

Further, removing the *right-shift* from $\tau_h^{Na_V1.2}$ stops backpropagation: In the ■$\tau_h^{Na_V1.2}$ curve of Fig 6B, all gating properties other than $\tau_h^{Na_V1.2}$, including $h_\infty^{Na_V1.2}$, retain their nominal *right-shift*, yet backpropagation ceases (according to our strict BAP criterion, see Section B in S1 Text) for axonal stimulation when $\Delta V_{RS} \lesssim -2\text{mV}$.

Table 1. Summary of sensitivity analysis: Impact of *right-shifted* $Na_V1.2$ gating properties in the AIS on backpropagation threshold (see Fig 6).

Type of Stimulation	● reference curve	Increasing ΔV_{RS} of *availability*			Increasing ΔV_{RS} of *activation*		
		■ $\tau_h^{Na_V1.2}$	◆ $h_\infty^{Na_V1.2}$	✚ $h_\infty^{Na_V1.2}$, $\tau_h^{Na_V1.2}$	✕ $\tau_m^{Na_V1.2}$	▲ $m_\infty^{Na_V1.2}$	▼ $m_\infty^{Na_V1.2}$, $\tau_m^{Na_V1.2}$
Axonal	↓	↓	↓	↓	↑(slight)	↑	↑
Somatic	↑	×	↓(slight)	↓(slight)	×	↑	↑

Arrows (↓,↑) indicate the sign of the **slopes** of backpropagation threshold curves in Fig 6A (somatic stimulation) and Fig 6B (axonal stimulation). A downward arrow (↓) indicates that the backpropagation threshold I_{BP} decreases with increasing *right-shift*, applied to the gating properties specified above it. Likewise, an upward arrow (↑) indicates that the threshold increases when the specified combination of $Na_V1.2$ variables is *right-shifted*. In cells marked "×" the effect of *right-shift* was negligible.

https://doi.org/10.1371/journal.pcbi.1011846.t001

For somatic stimulation, the *right-shifted activation* ($m^{Na_V1.2}$) drives I_{BP}. Travelling from right to left in Fig 6A, the most significant decrease in threshold occurs in the curves legended ▲$m_\infty^{Na_V1.2}$ and ▼$m_\infty^{Na_V1.2}$, $\tau_m^{Na_V1.2}$ as the nominal *right-shift* is removed ($\Delta V_{RS} \to -13.0\text{mV} \Rightarrow V_{RS} + \Delta V_{RS} \to 0$, see Fig P in S1 Text). The ▼$m_\infty^{Na_V1.2}$, $\tau_m^{Na_V1.2}$ curve differs negligibly from the ▲$m_\infty^{Na_V1.2}$ curve, showing that $m_\infty^{Na_V1.2}$ *right-shift* dominates in raising the threshold near the nominal point, and the *right-shift* of $\tau_m^{Na_V1.2}$ matters little.

Our ΔV_{RS} results from Fig 6 are summarized in Table 1.

Generalization to Hay-based model and modified Hu-based model

To demonstrate that our primary result—the separation of $Na_V1.2$ and $Na_V1.6$ into the proximal and distal AIS, respectively, promotes backpropagation with axonal stimulation but can *increase or decrease* I_{BP} with somatic stimulation—is not an artifact of our implementation of the model from Hu et al. (2009) [15] used thus far, we have inserted Na_V distributions analogous to Fig 1 into the model of Hay et al. (2011) [29] below. (Cell morphology in Fig B in S1 Text.)

(Also, in Section D in S1 Text, we include a modified version of the Hu-based model, with increased dendritic excitability and a less excitable soma. It has robust backpropagation in the entire dendritic tree without attenuation. Despite its 10× higher dendritic excitability, 3× lower somatic excitability, and qualitatively different backpropagation pattern, the results reported above are reproduced there as well.)

We replaced the single population of Na_Vs in the Hay model's 60μm AIS with two Na_V subtypes, based on their original Na_V kinetics: One population *left-shifted* by 6mV and the other *right-shifted* by 6mV, relative to the original $V_{1/2}$, to represent $Na_V1.6$ and $Na_V1.2$ respectively. Our manipulations of the Na_V channels' distribution (varying κ and x) did not change the total Na_V density in the AIS, which was kept identical to their model (https://modeldb.science/139653). Further, we attached an additional 400μm-long section of passive cable to the end of the AIS, where their axon originally stopped, to allow the AP to exit the AIS orthodromically as well as antidromically, as is the case in real neurons, in order to make AP generation in the Hay model more realistic. This was necessary to recover our qualitative results.

Our intention was to modify the Hay model as little as was necessary, since its parameters are tailored to a specific neuron and morphology—they will not necessarily transfer well even between specimens of the same cell type (see Hay et al. (2011) [29]). Presumably, the tuning may also be sensitive to the excitability of newly attached compartments.

We note that Hay et al. optimized their models to fit experimentally observed somatic and dendritic spiking patterns, including BAC firing, but their focus was not on action potential initiation. The models that best fit their data had AP initiation in the soma rather than the AIS, but they provide an additional model where APs were constrained to initiate in a 60μm section

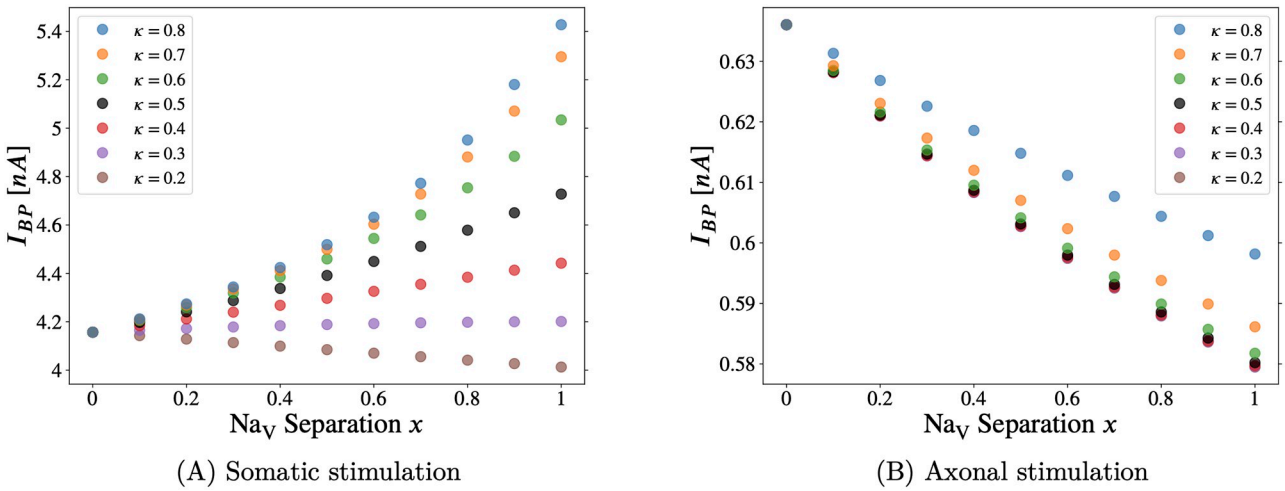

Fig 7. Backpropagation threshold in the Hay model: Combined effect on the backpropagation threshold (I_{BP}, defined below) of varying crossover location (κ) and Na_V separation (x) in the axon initial segment. Varying the separation parameter "x" from $x = 0$ to $x = 1$, the distribution of Na_V channels goes from flat (homogeneous) to separated, the latter approximating the distribution observed in developing pyramidal neurons (see Fig 1A, [20]). Note that curves for all values of κ converge to a single point at $x = 0$, since κ can have no effect when the two Na_V subtypes are uniformly distributed along the AIS. Apical dendrite backpropagation criterion $= -70.0\text{mV}$—see caption of Fig E in S1 Text. In the Hay model, the forward propagation threshold I_{FP} is not defined: There is no nowhere for saltatory conduction to occur, as there is no excitable axon beyond the AIS [29].

https://doi.org/10.1371/journal.pcbi.1011846.g007

named "axon", which had been set aside due to excessive BAP attenuation (see [29]). Since we required a parameter tuning with AP initiation in the AIS, the latter model was the necessary choice, despite its unrealistically strong attenuation of the backpropagated AP.

In Fig 7 we register backpropagation in the Hay model [29] as a depolarization of several mV in the apical dendrites, following current injection. Identical results using a somatic backpropagation measurement criterion are included as Fig F in S1 Text. The threshold was set at -70mV when measuring the depolarization near the bifurcation of the main apical dendrite, where $V_{\text{rest}} \cong -74.1\text{mV}$. See Fig E in S1 Text.

Note the qualitative agreement between the Hay-based model implemented and the Hu-based model above (and the modified Hu-based model in the Supporting Information (Section D in S1 Text)). In Fig 7A, we simulate backpropagation following somatic stimulation. As above in Fig 2 (and Fig H in S1 Text), concentrating $Na_V1.2$ in the proximal AIS tends to raise the backpropagation threshold, and increasing the proportion of total sodium conductance in the AIS allocated to $Na_V1.6$ lowers I_{BP}.

In Fig 7B, we simulate backpropagation following axonal stimulation. As above in Figs 4 and 5 (and Fig J in S1 Text), the separated Na_V distribution ($x \to 1$) lowers the threshold in the Hay model. Quantitatively, Fig 7B is closer to Fig 5, suggesting that the concentration of low-threshold $Na_V1.6$ at the distal AIS, rather than the concentration of $Na_V1.2$ at the proximal AIS, promotes backpropagation. What is important to keep in mind is that, in both models, concentrating $Na_V1.2$ in the proximal AIS only lowered I_{BP} in the case of depolarizing axonal current injection.

Rescaling the $Na_V1.2$ density profile by a uniform factor in the AIS

In this section, we rescale the $Na_V1.2$ density profile in the Hay-based model via the maximal conductance $\bar{g}_{Na_V1.2}$. At each segment of the AIS, $\bar{g}_{Na_V1.2}$ is multiplied by a positive number

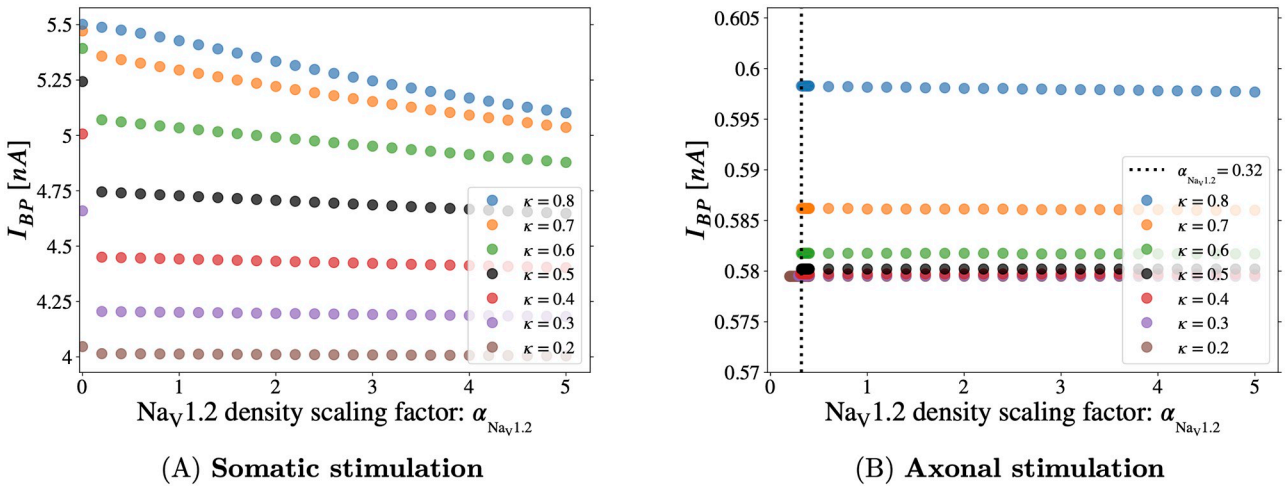

Fig 8. Scaling the $Na_V1.2$ density profile in the AIS of the Hay-based model [29], with somatic vs. axonal stimulation. The backpropagation threshold is computed while the local $Na_V1.2$ density is rescaled by $\alpha_{Na_V1.2}$ at every AIS segment. Here we have set $x = 1$ so that the $Na_V1.2$ and $Na_V1.6$ density profiles are separated, guaranteeing that the proximal AIS is exclusively populated with $Na_V1.2$—see Fig 1. With somatic stimulation **(A)**, backpropagation persists even when $Na_V1.2$ is completely removed from the AIS ($\alpha_{Na_V1.2} = 0$). However, with axonal stimulation **(B)**, backpropagation ends abruptly near $\alpha_{Na_V1.2} \lesssim 0.32$. Yet again, the importance of the proximal $Na_V1.2$ subtype and its qualitative effects on excitability depend heavily on the mode of stimulation. Density of data points is increased near the vertical dashed line to detect backpropagation cutoff.

https://doi.org/10.1371/journal.pcbi.1011846.g008

which we call the $Na_V1.2$ scaling factor, denoted $\alpha_{Na_V1.2}$. That is, at each point s in the AIS,

$$\bar{g}_{Na_V1.2}(s) \rightarrow \alpha_{Na_V1.2}\bar{g}_{Na_V1.2}(s), \tag{4}$$

with $\alpha_{Na_V1.2} \geqslant 0$. In Fig 8A the backpropagation threshold is computed with somatic current injection (see Fig E in S1 Text). We observe that reducing the density of $Na_V1.2$, without adding any compensatory $Na_V1.6$ density, increases the threshold as expected—the slope is most visible on the $\kappa = 0.8$ line of Fig 8A, wherein the majority of the AIS (except the most distal region, see Fig 1B) contains $Na_V1.2$ and is therefore affected by $\alpha_{Na_V1.2}$. Even when $Na_V1.2$ is completely removed from the AIS, and consequently the proximal AIS contains no Na_V channels, backpropagation is possible with somatic stimulation.

In Fig 8B it is interesting to see, yet again, the sharp qualitative difference in the role of the $Na_V1.2$ subtype with axonal versus somatic stimulation. As noted above, backpropagation is present in Fig 8A when the AIS $Na_V1.2$ channels are disabled entirely ($\alpha_{Na_V1.2} = 0$). With axonal stimulation however (Fig 8B), the effect of $\alpha_{Na_V1.2}$ was abrupt and binary, akin to a Heaviside function. I_{BP} was nearly flat, except the Hay neuron did not produce a BAP when $\alpha_{Na_V1.2} \lesssim 0.32$—some nonzero Na_V density was required in the proximal AIS for backpropagation.

With somatic stimulation, the neuron is primed for backpropagation by the electrode current, which depolarizes the soma before the AP arrives from the AIS. As $\alpha_{Na_V1.2} \rightarrow 0$, increased somatic stimulation can compensate for the resulting loss of depolarizing Na_V current from the proximal AIS.

With axonal stimulation, there is no direct pre-charging of the soma by the injected current pulse. When $\alpha_{Na_V1.2}$ decreases the density of channels at the proximal AIS, the electrode cannot compensate for the lost $Na_V1.2$ current, due to its electrical isolation from the soma. The abrupt BAP cutoff reflects the all-or-none nature of action potentials. The lack of slope in I_{BP}

owes to the fact that the axonal current pulse depolarizes the most distal end of the AIS, which sets the threshold in this case [15] (provided the proximal Na_V density is sufficient, see above). The distal AIS is populated exclusively by $Na_V1.6$ channels, and hence it is unaffected by $\alpha_{Na_V1.2}$.

Discussion

In early development, pyramidal neurons concentrate $Na_V1.2$ in the proximal AIS, and $Na_V1.6$ in the distal AIS. As these cells mature, $Na_V1.6$ invades the proximal AIS, and the two Na_V subtypes lose their separated distribution [20]. We have investigated the effects of Na_V separation in the axon initial segment on the initiation and backpropagation of action potentials in three different pyramidal neuron models. In spite of their different parameters, axonal and dendritic morphology, and biophysics, all three models (see: Somatic stimulation, Axonal stimulation, Modifying the *right-shift* of $Na_V1.2$ gating properties in the AIS, Generalization to Hay-based model and modified Hu-based model, and Section D in S1 Text) indicated that the effects of the separated Na_V distribution depend on whether stimulation is orthodromic (e.g. somatodendritic input) or antidromic (e.g. axonal stimulation).

With somatic stimulation, the greater the proportion of $Na_V1.2$ in the AIS, relative to $Na_V1.6$, the less excitable the cell becomes (increased I_{BP}). Our somatic current injection results are contrary to past modelling which used axonal stimulation [15], although they are consistent with more recent experimental results that used somatic stimulation [18]. The threshold-raising effect of proximal $Na_V1.2$ is confirmed by repeating the simulations with a model cell in which the AIS has been flipped longitudinally (Fig 3), placing $Na_V1.6$ proximally and $Na_V1.2$ distally in the AIS.

Our results using axonal stimulation agree qualitatively with and expand upon past modelling efforts [15]: In all three models, with axonal current injection, excitability is greatest (lowest I_{BP}) when Na_V subtypes are separated in the AIS ('*x*-shaped distribution'). Further, in the Hu-based models (Fig 4, Fig J in S1 Text), increasing the total proportion of $Na_V1.2$ in the AIS —by moving the Na_V crossover κ distally—promotes backpropagation as well. In the Hay-based model, removing Na_Vs from the proximal AIS halted backpropagation. We also find that increased distal $Na_V1.6$ concentration (which results from the separated distribution) lowers the AP threshold (Fig 5).

Testing both modes of stimulation can contribute to resolving inconsistencies between experiments such as [18] and [15], where stimulation was orthodromic in the former and antidromic in the latter. In [18], AP initiation was observed in pyramidal neurons which were engineered to be $Na_V1.6$-deficient. In those neurons, the AIS was populated entirely with $Na_V1.2$, however they still found that the AIS Na_V current was *left-shifted* relative to the somatic current. From this and other observations, the authors in [18] suggest that the distribution of Na_V subtypes is not so important in shifting the local voltage-gated Na^+ current.

We note that, compared to control neurons, the $Na_V1.6$-deficient neurons' AIS Na_V current was *right-shifted*, and the orthodromic AP threshold (amplitude of a 2ms current pulse [18]) was nearly doubled. This is consistent with our results and the modelling assumption that *right-shift* is associated with $Na_V1.2$ in the AIS—the model is agnostic about the molecular details. The decrease in excitability reported in [18] may have been even larger had they used more mature neurons. Their neurons were obtained from 4–5 week old mice, at which point the AIS will still be largely populated with $Na_V1.2$, whereas in wild type mice $Na_V1.6$ replaces much of the $Na_V1.2$ by 90 days [20, 30]. Our results indicate that with axonal stimulation, $Na_V1.6$-deficient cells may have a lower backpropagation threshold than the wild type.

The loss of the separated Na_V distribution in the AIS at later developmental stages, accompanied by the proximal localization of $Na_V1.6$, may enhance excitability to healthy orthodromic stimulation while protecting against the backpropagation of ectopic activity from damaged axons into the soma and dendrites. Further, research into the genetic causes of autism spectrum disorder has revealed that $Na_V1.2$ knockout can enhance pyramidal cells' tendency to send action potentials and simultaneously reduce backpropagation (somatodendritic hypoexcitability) [19]. Whereas [19] reported an interplay between $Na_V1.2$ and K_V, in contrast, our results are explained by the spatial distribution of Na_V *right-shift* within the AIS (Table 1, Fig 6A). Indeed, the reduced excitability resulting from AIS $Na_V1.2$ owes to the asymmetric impact of *availability* on backpropagation in axonal versus somatic stimulation (Fig 6).

Although *right-shifting* $Na_V1.2$ steady-state *availability*, $h_\infty^{Na_V1.2}(V)$, in the AIS is necessary to promote backpropagation (i.e. decrease I_{BP}) when stimulation is axonal, it is not sufficient on its own. Our modelling shows that the voltage-sensitive time constant of *availability*, $\tau_h^{Na_V1.2}(V)$, must be *right-shifted* as well (Fig 6B, ■$\tau_h^{Na_V1.2}$ curve).

It is straightforward to explain why increasing ΔV_{RS} lowers I_{BP} in the ◆$h_\infty^{Na_V1.2}$ curves of Fig 6A and 6B: *Right-shifting* steady-state $Na_V1.2$ *availability* increases Na^+ conductance at all voltages because $h_\infty^{Na_V1.2}(V)$ is monotonically decreasing (Fig Pi in S1 Text). However, without sensitivity analysis, it was *not* obvious that removing the nominal *right-shift* from the voltage-sensitive time constant $\tau_h^{Na_V1.2}$—without modifying steady-state *activation* ($m_\infty^{Na_V1.2}$) or *availability* ($h_\infty^{Na_V1.2}$)—would on its own be sufficient to eliminate the I_{BP}-lowering effects of $Na_V1.2$ for axonal stimulation. This effect is demonstrated in the curve legended ■$\tau_h^{Na_V1.2}$ of Fig 6B. It follows that the *x*-distribution's tendency to promote backpropagation is not merely a result of increased steady-state *availability* of proximal AIS Na_Vs, but is a dynamic effect—dependent on the *right-shift* of $\tau_h^{Na_V1.2}(V)$ as well.

From Fig Pii in S1 Text, we can see that *right-shifting* $Na_V1.2$ slows down the *inactivation* process via its time constant—which is the voltage-sensitive time constant of *availability*. The membrane potential traverses the $\tau_h^{Na_V1.2}(V)$ curve during an AP. *Right-shifting* $\tau_h^{Na_V1.2}(V)$ moves the maximum value of the time constant to depolarized voltages, and slows down *inactivation* so that more channels are *available* to assist with backpropagation.

There is an interplay between cable properties and the distribution of Na_Vs in determining the site of AP initiation [44]. Electrical isolation of the initiation site may amplify the effect of concentrating $Na_V1.6$ in the distal AIS. Via fluorescence imaging of intracellular Na^+ concentration following single action potentials, [35] located the greatest Na^+ influx at the middle of the AIS, whereas the distal AIS (initiation site) had only 1/4 of this maximum. They inferred that the density of Na_V channels decreases toward the initiation site, and thus Na_V density does not determine the precise location where APs begin.

Although [35] did not require $Na_V1.6$ accumulation at the distal AIS to explain the distal location of the initiation site, the authors suggest that local Na_V density can have a large effect on neuronal excitability. Temperature may also play a role in local AIS Na^+ influx measurements due to the spatial separation of Na_V subtypes. The pyramidal neurons in [35] and [18] were cooled to $\cong 21^\circ$, and $Na_V1.2$ and $Na_V1.6$ differ in their responses to temperature changes [17]. Thus, a deeper exploration of the effects of temperature on AP initiation is warranted.

The temporal resolution of Na^+ influx measurements continues to improve: [45] achieved a resolution of 0.1ms imaging pyramidal cells in mouse brain slices. Another order of magnitude improvement may be sufficient to discern the local contributions of Na_V subtypes to AP initiation. The qualitative dependence of the backpropagation threshold on the somatic-versus-axonal mode of stimulation is compatible with distal AP generation as found in [15, 35] and in our work, but does not seem to rely crucially on the precise determinants of AP onset

position; it relies rather on the *activation* and *availability* properties, and the kinetics of the latter.

The effect of realistic synaptic input is a broad interesting question that is beyond the scope of this study. Furthermore, including it at this point would defeat the purpose of comparing axonal versus somatic stimulation, since antidromic axonal input will be in the form of a brief pulse (no excitatory synaptic input typically occurs onto axons of pyramidal neurons, and when it does it generates an AP). Because our simulations compare orthodromic stimulation to antidromic stimulation, the shape of the injected current must be kept identical in each mode to isolate the effect of the Na_V density profiles on I_{BP}.

We would expect that fast glutamatergic input near the soma, or propagating to the soma from sufficiently synchronized dendritic synaptic inputs, would yield qualitatively similar results as reported here. There may be qualitative changes if the synaptic input has a slower rise time, e.g. for synapses with a large NMDA component.

Since the Na_V distribution changes throughout development, a further investigation—beyond the scope of this paper, as we will explain—would be to understand how accompanying developmental changes in morphological complexity and voltage-gated channel density elsewhere in the neuron [46] interact with developmental plasticity in the AIS. This would require new parameter sets at each iteration of the morphological complexity. Since Hay et al. [29] had to fit each morphology's parameter set to match firing patterns observed in real neurons, that procedure would need to be repeated. If sufficient experimental data are not available to perform the fitting at each iteration, new electrophysiological experiments would be necessary at the corresponding developmental stages. That endeavour is beyond the scope of the present study. Also, there is experimental evidence that AIS plasticity is not limited to development [6]. Our strategy was to restrict our investigation to the effects of varying the heterogeneous distribution of Na_V subtypes in the AIS on backpropagation threshold, with different modes of stimulation. Note, that the changing Na_V distributions we simulate are not strictly intended to replicate observed plasticity. Even if the Na_V distribution in the AIS of real neurons were static, modelling the hypothetical distributions would nonetheless assist in understanding its function via the resulting changes to cellular excitability.

Our model neurons were kept identical in all results presented above; only the AIS was altered. Our results therefore can only be explained by the distribution of Na_V subtypes (or, the distribution of *right-shifted* Na_V gating properties) within the AIS. Given the τ_h-dependence of the antidromic backpropagation threshold in Modifying the *right-shift* of $Na_V1.2$ gating properties in the AIS, and the differential temperature sensitivity of $Na_V1.2$ versus $Na_V1.6$ [17], there is good reason to expect that the effects of Na_V separation predicted here will be temperature-dependent.

In summary, we have simulated a range of hypothetical Na_V distributions in the axon initial segment of three 3D-reconstructed biophysical pyramidal cell models, including two distinct morphologies and three different parameter tunings. Our modelling shows that the spatial profile of $Na_V1.2$ and $Na_V1.6$ in the AIS and the kinetics of their *availability* and *activation* are important determinants of excitability and the backpropagation threshold. We predict that the separation of Na_V subtypes observed in early development has an asymmetrical effect on excitability which depends on whether the neuron is stimulated orthodromically or antidromically. With orthodromic stimulation, Na_V separation impedes backpropagation and reduces excitability unless the crossover is brought close to the soma. Backpropagation and excitability are both enhanced by Na_V separation when stimulation is antidromic. Maintaining a static Na_V distribution, we altered the *right-shift* of selected $Na_V1.2$ gating properties. This revealed that steady-state *activation right-shift* controls the orthodromic backpropagation threshold, and dynamic *availability right-shift* is necessary to explain the antidromic threshold. Furthermore,

given that learning is linked to backpropagation, the evolving separation of the Na_V subtypes may impact synaptic weight modification across developmental stages.

Materials and methods

The pyramidal cell models (Figs A and B in S1 Text) were implemented in NEURON 8.0 [47] via Python. For cell geometry, local membrane properties, additional simulations, and a variety of calculations, clarifications, and definitions, see S1 Text, which has its own table of contents.

Our Hay-based model is biophysically and morphologically identical to the original [29], aside from the modified *right-shift* in axonal Na_V channels that we introduced to create $Na_V1.2$ and $Na_V1.6$ variants in the AIS, and an additional passive section attached to the end of the axon. Our implementation of the Hay model (https://modeldb.science/139653) is detailed in Generalization to Hay-based model and modified Hu-based model.

Our Hu-based model [15] uses the same reconstructed morphology as the original model (https://modeldb.science/123897), which is a Layer 5 pyramidal neuron from cat visual cortex, modified from [26] (see SI, Section A in S1 Text). We added explicit intracellular and extracellular concentrations of sodium, potassium, and chloride ions. Because of this change, the Nernst potentials E_{Na^+}, E_{K^+}, E_{Cl^-} are calculated locally from each compartment's specific ionic concentrations, which respond to transmembrane currents. The $Na_V1.2$, $Na_V1.6$, and K_V kinetics from [15] are included as well.

We also included active transport via a Na^+/K^+-pump current, to maintain the transmembrane concentration gradients of Na^+ and K^+. In our Hu-based model, all ions are subject to longitudinal diffusion, both intra- and extracellular, implemented using NEURON's RxD facility [48, 49]. The cell maintains a resting potential $V_{rest} \cong -70\text{mV}$ at steady-state, and restores this state following stimulation. The biophysics that governs local ion concentrations (and Nernst potentials) in the Hu-based model is summarized in Biophysics, Hu-based model.

AIS—Na_V density profiles

In all of the models presented in this study, the density profiles of $Na_V1.2$ and $Na_V1.6$ are left- and right-handed sigmoidal functions (respectively) of normalized length s along the AIS. The proximal end of the AIS is located at $s = 0$, and the distal end is located at $s = 1$. The channel densities are expressed as maximal conductances $\bar{g}_{Na_V1.6}$ (s) and $\bar{g}_{Na_V1.2}$ (s), where the total maximal Na_V conductance $\bar{g}_{Na_V}$ is constant along the AIS:

$$\bar{g}_{Na_V} = \bar{g}_{Na_V1.2}(s) + \bar{g}_{Na_V1.6}(s) = \text{const.} \tag{5}$$

The density profiles are given by

$$\begin{cases} \bar{g}_{Na_V1.2}(s) & = \dfrac{\bar{g}_{Na_V}}{2}\left(1 - x \cdot \tanh(\sigma(s-\kappa))\right), \\ \bar{g}_{Na_V1.6}(s) & = \bar{g}_{Na_V} - \bar{g}_{Na_V1.2}(s) \\ & = \dfrac{\bar{g}_{Na_V}}{2}\left(1 + x \cdot \tanh(\sigma(s-\kappa))\right). \end{cases} \tag{6}$$

We chose the hyperbolic tangent function $\tanh(s)$, but other sigmoidal functions would do just as well. The parameter x controls the separation of the Na_V distribution, that is, how separated the two Na_V subtypes are. When $x = 0$, the distribution becomes flat—$Na_V1.2$ and $Na_V1.6$ are mixed uniformly along the AIS. When $x = 1$, the proximal end of the AIS contains only $Na_V1.2$, and the distal end of the AIS contains only $Na_V1.6$. The parameter σ is the reciprocal

of the 'transition width' of the AIS Na_V distributions normalized by the AIS length. In all simulations shown here, $\sigma = 10.0$. Additional details are provided in Section E in S1 Text.

Shift-Clamping and the Hodgkin-Huxley model

Here we provide additional details of the sensitivity analysis performed in Fig 6. In the Hodgkin-Huxley model [40] a gating variable u evolves according to its voltage-dependent forward and backward transition rates $\alpha_u(V)$ and $\beta_u(V)$ as

$$\frac{du}{dt} = \alpha_u(V)[1-u] - \beta_u(V)u, \tag{7}$$

where u could be Na_V *activation m* or *availability h*, or K_V *activation n*, etc. This can be rewritten using the steady-state $u_\infty(V)$ and voltage-dependent time constant $\tau_u(V)$ of the gating variable

$$\frac{du}{dt} = \frac{u_\infty(V) - u}{\tau_u(V)}, \tag{8}$$

where u_∞ and τ_u are computed from α_u and β_u via

$$u_\infty(V) = \frac{\alpha_u(V)}{\alpha_u(V)+\beta_u(V)} \quad \text{and} \quad \tau_u(V) = \frac{1}{\alpha_u(V)+\beta_u(V)} \quad . \tag{9}$$

When shifting the voltage-dependence of u_∞ by ΔV_{RS} (see Modifying the *right-shift* of $Na_V1.2$ gating properties in the AIS), it is natural to assume that one should apply the same shift to τ_u given Eq 9, since u_∞ and τ_u are both functions of $\alpha_u(V)$ and $\beta_u(V)$ in such models. However, our simulations can shift $u_\infty(V)$ or $\tau_u(V)$ independently of one another: e.g. $\tau'_u(V) = \tau_u(V - \Delta V_{RS})$, $u'_\infty(V) = u_\infty(V)$. The forward and backward rates become

$$\alpha'_u = \frac{u'_\infty(V)}{\tau'_u(V)} \quad \text{and} \quad \beta'_u = \frac{1-u'_\infty(V)}{\tau'_u(V)}. \tag{10}$$

Putting this to use, one can modify the *right-shift* of combinations of

$$\left\{\tau_h^{Na_V1.2}(V),\ h_\infty^{Na_V1.2}(V),\ \tau_m^{Na_V1.2}(V),\ m_\infty^{Na_V1.2}(V)\right\}, \tag{11}$$

by adding "$-\Delta V_{RS}$" to the argument of the selected variables' $u_\infty(V)$s or $\tau_u(V)$s.

Biophysics, Hu-based model

Action potentials propagate via the cable equation

$$C\frac{\partial V}{\partial t} = \frac{d}{4R_a}\frac{\partial^2 V}{\partial s^2} - I_{\text{membrane}}, \tag{12}$$

where V is the membrane potential, C is the specific membrane capacitance, d is the neurite diameter, R_a is the axial resistance, s is the position along the axis of the cable, and I_{membrane} is the total transmembrane current density of all ion species in the model.

Here we describe the currents in our Hu-based model. (The changes we made to the Hay model are described in Generalization to Hay-based model and modified Hu-based model.) In the Hu-based model, we added explicit intracellular and extracellular concentrations of sodium, potassium, and chloride ions at each compartment. We denote the intracellular/extracellular concentration of a given ionic species "Z" as $[Z]_{in}$, $[Z]_{out}$ respectively. These

concentrations depend on the spatial coordinate—i.e. $[Z]_{in} = [Z]_{in}(s)$—but that is not written explicitly, to simplify the notation. The Nernst potentials (reversal potentials) E_{Na^+}, E_{K^+}, E_{Cl^-} of Na^+, K^+, and Cl^- are not fixed parameters but are instead determined by the intracellular and extracellular concentrations of those ions:

$$E_Z(s) = -\frac{kT}{q_z}\ln\left(\frac{[Z]_{in}}{[Z]_{out}}\right). \tag{13}$$

Transmembrane concentration gradients of Na^+ and K^+ are governed by active transport (Na^+/K^+-pump) and longitudinal diffusion. At each time step, ionic concentrations all over the cell are updated using transmembrane currents (Eq 16) and Fick's law. At the j^{th} compartment this gives:

$$\begin{cases} \frac{\partial}{\partial t}[Z]^j_{in} = -\left(\frac{A^j}{FVol^j_{in}}\right) I^j_Z + D_Z\nabla^2[Z]^j_{in} \\ \\ \frac{\partial}{\partial t}[Z]^j_{out} = \left(\frac{A^j}{FVol^j_{out}}\right) I^j_Z + D_Z\nabla^2[Z]^j_{out}, \end{cases} \tag{14}$$

where I^j_Z is the transmembrane current density of ion species Z at compartment j, with $Z = Cl^-$, K^+, Na^+. D_Z denotes the diffusion coefficient of ion Z. A^j and $Vol^j_{in(out)}$ are (respectively) the membrane area and intracellular/extracellular volume at the j^{th} compartment. F is the Faraday constant. The total transmembrane current density at the j^{th} compartment is

$$I^j_{membrane} = I^j_{Cl^-} + I^j_{K^+} + I^j_{Na^+}. \tag{15}$$

Omitting the compartment index j, the specific transmembrane currents are

$$I_{membrane} \leftarrow \begin{cases} I_{Cl^-} = g_{Cl^-}(V - E_{Cl^-}) \\ I_{K^+} = (g_{K_V} + g_{K,leak})(V - E_{K^+}) - 2I_{pump} \\ I_{Na^+} = (g_{Na_V} + g_{Na,leak})(V - E_{Na^+}) + 3I_{pump}. \end{cases} \tag{16}$$

g_{Cl^-}, $g_{K,leak}$, and $g_{Na,leak}$ are passive leak conductances whereas g_{K_V} and g_{Na_V} have voltage-gated Hodgkin-Huxley (HH)-style kinetics (Eq S6 in S1 Text). Since channels are nonuniformly distributed along the cell membrane, conductances vary with location. I_{pump} is the net current produced by the Na^+/K^+-pump as a function of $[K^+]_{out}$ and $[Na^+]_{in}$,

$$I_{pump} = I_{maxpump}\left(1 + \frac{K_{M_{K^+}}}{[K^+]_{out}}\right)^{-2}\left(1 + \frac{K_{M_{Na^+}}}{[Na^+]_{in}}\right)^{-3}, \tag{17}$$

where $I_{maxpump}$ controls the maximal pump current, $K_{M_{K^+}}$ and $K_{M_{Na^+}}$ are Michaelis-Menten kinetic constants, and the Na^+ and K^+ currents flowing through the pump are $I_{Na^+,pump} = 3I_{pump}$ and $I_{K^+,pump} = -2I_{pump}$. (Calcium dynamics are omitted in this section since Hu et al. [15] did not include the dendritic calcium spike initiation zone—see [39]. In Generalization to Hay-based model and modified Hu-based model, we include the Hay model, which features state-of-the-art calcium dynamics.).

Supporting information

S1 Text. For cell geometry, local membrane properties, additional simulations, and a variety of calculations, clarifications, and definitions, see this file.
(PDF)

Acknowledgments

We wish to thank: Catherine E. Morris, for directing our attention to the AIS. Nicholas T. Carnevale and Robert A. McDougal, for generously helping us to solve a number of model implementation challenges using NEURON. We also thank Louis Jacques for helpful discussion.

Author Contributions

Conceptualization: Benjamin S. M. Barlow, André Longtin, Béla Joós.

Formal analysis: Benjamin S. M. Barlow, André Longtin, Béla Joós.

Funding acquisition: André Longtin, Béla Joós.

Investigation: Benjamin S. M. Barlow, André Longtin, Béla Joós.

Methodology: Benjamin S. M. Barlow, André Longtin, Béla Joós.

Project administration: André Longtin, Béla Joós.

Resources: André Longtin, Béla Joós.

Software: Benjamin S. M. Barlow.

Supervision: André Longtin, Béla Joós.

Validation: Benjamin S. M. Barlow, André Longtin, Béla Joós.

Visualization: Benjamin S. M. Barlow.

Writing – original draft: Benjamin S. M. Barlow.

Writing – review & editing: Benjamin S. M. Barlow, André Longtin, Béla Joós.

References

1. Debanne D, Campanac E, Bialowas A, Carlier E, Alcaraz G. Axon Physiology. Physiological Reviews. 2011; 91(2):555–602. https://doi.org/10.1152/physrev.00048.2009 PMID: 21527732
2. Adachi R, Yamada R, Kuba H. Plasticity of the Axonal Trigger Zone. Neuroscientist. 2015; 21(3):255–265. https://doi.org/10.1177/1073858414535986 PMID: 24847046
3. Gulledge AT, Bravo JJ. Neuron Morphology Influences Axon Initial Segment Plasticity. eNeuro. 2016; 3 (1). https://doi.org/10.1523/ENEURO.0085-15.2016 PMID: 27022619
4. Verbist C, Müller MG, Mansvelder HD, Legenstein R, Giugliano M. The location of the axon initial segment affects the bandwidth of spike initiation dynamics. PLOS Computational Biology. 2020; 16(7): e1008087. https://doi.org/10.1371/journal.pcbi.1008087 PMID: 32701953
5. Franken TP, Bondy BJ, Haimes DB, Goldwyn JH, Golding NL, Smith PH, et al. Glycinergic axonal inhibition subserves acute spatial sensitivity to sudden increases in sound intensity. eLife. 2021; 10:e62183. https://doi.org/10.7554/eLife.62183 PMID: 34121662
6. Petersen AV, Cotel F, Perrier JF. Plasticity of the Axon Initial Segment: Fast and Slow Processes with Multiple Functional Roles. Neuroscientist. 2017; 23(4):364–373. https://doi.org/10.1177/1073858416648311 PMID: 27143656
7. Vrselja Z, Daniele SG, Silbereis J, Talpo F, Morozov YM, Sousa AMM, et al. Restoration of brain circulation and cellular functions hours post-mortem. Nature. 2019; 568(7752):336–343. https://doi.org/10.1038/s41586-019-1099-1 PMID: 30996318

8. Shepherd GM, Marenco L, Hines ML, Migliore M, McDougal RA, Carnevale NT, et al. Neuron Names: A Gene- and Property-Based Name Format, With Special Reference to Cortical Neurons. Frontiers in Neuroanatomy. 2019; 13. https://doi.org/10.3389/fnana.2019.00025 PMID: 30949034
9. Kole MHP, Stuart GJ. Signal Processing in the Axon Initial Segment. Neuron. 2012; 73(2):235–247. https://doi.org/10.1016/j.neuron.2012.01.007 PMID: 22284179
10. Höfflin F, Jack A, Riedel C, Mack-Bucher J, Roos J, Corcelli C, et al. Heterogeneity of the Axon Initial Segment in Interneurons and Pyramidal Cells of Rodent Visual Cortex. Frontiers in Cellular Neuroscience. 2017; 11:332. https://doi.org/10.3389/fncel.2017.00332
11. Shu Y, Duque A, Yu Y, Haider B, McCormick DA. Properties of Action-Potential Initiation in Neocortical Pyramidal Cells: Evidence From Whole Cell Axon Recordings. Journal of Neurophysiology. 2007; 97 (1):746–760. https://doi.org/10.1152/jn.00922.2006 PMID: 17093120
12. Mainen ZF, Joerges J, Huguenard JR, Sejnowski TJ. A model of spike initiation in neocortical pyramidal neurons. Neuron. 1995; 15(6):1427–1439. https://doi.org/10.1016/0896-6273(95)90020-9 PMID: 8845165
13. Kole MHP, Ilschner SU, Kampa BM, Williams SR, Ruben PC, Stuart GJ. Action potential generation requires a high sodium channel density in the axon initial segment. Nat Neurosci. 2008; 11(2):178–186. https://doi.org/10.1038/nn2040 PMID: 18204443
14. Brette R. Sharpness of Spike Initiation in Neurons Explained by Compartmentalization. PLOS Computational Biology. 2013; 9(12):e1003338. https://doi.org/10.1371/journal.pcbi.1003338 PMID: 24339755
15. Hu W, Tian C, Li T, Yang M, Hou H, Shu Y. Distinct contributions of Nav1.6 and Nav1.2 in action potential initiation and backpropagation. Nat Neurosci. 2009; 12(8):996–1002. https://doi.org/10.1038/nn.2359 PMID: 19633666
16. Tian C, Wang K, Ke W, Guo H, Shu Y. Molecular identity of axonal sodium channels in human cortical pyramidal cells. Front Cell Neurosci. 2014; 8. https://doi.org/10.3389/fncel.2014.00297 PMID: 25294986
17. Ye M, Yang J, Tian C, Zhu Q, Yin L, Jiang S, et al. Differential roles of NaV1.2 and NaV1.6 in regulating neuronal excitability at febrile temperature and distinct contributions to febrile seizures. Sci Rep. 2018; 8(1):753. https://doi.org/10.1038/s41598-017-17344-8 PMID: 29335582
18. Katz E, Stoler O, Scheller A, Khrapunsky Y, Goebbels S, Kirchhoff F, et al. Role of sodium channel subtype in action potential generation by neocortical pyramidal neurons. PNAS. 2018; 115(30):E7184–E7192. https://doi.org/10.1073/pnas.1720493115 PMID: 29991598
19. Spratt PWE, Alexander RPD, Ben-Shalom R, Sahagun A, Kyoung H, Keeshen CM, et al. Paradoxical hyperexcitability from NaV1.2 sodium channel loss in neocortical pyramidal cells. Cell Reports. 2021; 36(5). https://doi.org/10.1016/j.celrep.2021.109483 PMID: 34348157
20. Liu H, Wang HG, Pitt G, Liu Z. Direct Observation of Compartment-Specific Localization and Dynamics of Voltage-Gated Sodium Channels. J Neurosci. 2022; 42(28):5482–5498. https://doi.org/10.1523/JNEUROSCI.0086-22.2022 PMID: 35672149
21. Rush AM, Dib-Hajj SD, Waxman SG. Electrophysiological properties of two axonal sodium channels, $Na_v1.2$ and $Na_v1.6$, expressed in mouse spinal sensory neurones: Sodium channels in sensory neurones. The Journal of Physiology. 2005; 564(3):803–815. https://doi.org/10.1113/jphysiol.2005.083089 PMID: 15760941
22. Wang JA, Lin W, Morris T, Banderali U, Juranka PF, Morris CE. Membrane trauma and Na+ leak from Nav1.6 channels. American Journal of Physiology-Cell Physiology. 2009; 297(4):C823–C834. https://doi.org/10.1152/ajpcell.00505.2008 PMID: 19657055
23. Ben-Shalom R, Keeshen CM, Berrios KN, An JY, Sanders SJ, Bender KJ. Opposing Effects on Na V 1.2 Function Underlie Differences Between SCN2A Variants Observed in Individuals With Autism Spectrum Disorder or Infantile Seizures. Biological Psychiatry. 2017; 82(3):224–232. https://doi.org/10.1016/j.biopsych.2017.01.009 PMID: 28256214
24. Feldman D. The Spike-Timing Dependence of Plasticity. Neuron. 2012; 75(4):556–571. https://doi.org/10.1016/j.neuron.2012.08.001 PMID: 22920249
25. Regehr WG, Carey MR, Best AR. Activity-Dependent Regulation of Synapses by Retrograde Messengers. Neuron. 2009; 63(2):154–170. https://doi.org/10.1016/j.neuron.2009.06.021 PMID: 19640475
26. Mainen ZF, Sejnowski TJ. Influence of dendritic structure on firing pattern in model neocortical neurons. Nature. 1996; 382(6589):363–366. https://doi.org/10.1038/382363a0 PMID: 8684467
27. Doiron B, Longtin A, Turner RW, Maler L. Model of Gamma Frequency Burst Discharge Generated by Conditional Backpropagation. Journal of Neurophysiology. 2001; 86(4):1523–1545. https://doi.org/10.1152/jn.2001.86.4.1523 PMID: 11600618
28. Larkum ME, Kaiser KMM, Sakmann B. Calcium electrogenesis in distal apical dendrites of layer 5 pyramidal cells at a critical frequency of back-propagating action potentials. Proc Natl Acad Sci USA. 1999; 96(25):14600–14604. https://doi.org/10.1073/pnas.96.25.14600 PMID: 10588751

29. Hay E, Hill S, Schürmann F, Markram H, Segev I. Models of Neocortical Layer 5b Pyramidal Cells Capturing a Wide Range of Dendritic and Perisomatic Active Properties. PLoS Comput Biol. 2011; 7(7): e1002107. https://doi.org/10.1371/journal.pcbi.1002107 PMID: 21829333

30. Spratt PWE, Ben-Shalom R, Keeshen CM, Burke KJ, Clarkson RL, Sanders SJ, et al. The Autism-Associated Gene Scn2a Contributes to Dendritic Excitability and Synaptic Function in the Prefrontal Cortex. Neuron. 2019; 103(4):673–685.e5. https://doi.org/10.1016/j.neuron.2019.05.037 PMID: 31230762

31. Payeur A, Guerguiev J, Zenke F, Richards BA, Naud R. Burst-dependent synaptic plasticity can coordinate learning in hierarchical circuits. Nat Neurosci. 2021; 24(7):1010–1019. https://doi.org/10.1038/s41593-021-00857-x PMID: 33986551

32. Fletcher LN, Williams SR. Neocortical Topology Governs the Dendritic Integrative Capacity of Layer 5 Pyramidal Neurons. Neuron. 2019; 101(1):76–90.e4. https://doi.org/10.1016/j.neuron.2018.10.048 PMID: 30472076

33. Beaulieu-Laroche L, Brown NJ, Hansen M, Toloza EHS, Sharma J, Williams ZM, et al. Allometric rules for mammalian cortical layer 5 neuron biophysics. Nature. 2021; 600(7888):274–278. https://doi.org/10.1038/s41586-021-04072-3 PMID: 34759318

34. Beaulieu-Laroche L, Toloza EHS, Van Der Goes MS, Lafourcade M, Barnagian D, Williams ZM, et al. Enhanced Dendritic Compartmentalization in Human Cortical Neurons. Cell. 2018; 175(3):643–651. e14. https://doi.org/10.1016/j.cell.2018.08.045 PMID: 30340039

35. Baranauskas G, David Y, Fleidervish IA. Spatial mismatch between the Na+ flux and spike initiation in axon initial segment. PNAS. 2013. https://doi.org/10.1073/pnas.1215125110 PMID: 23341597

36. Michalikova M, Remme MWH, Kempter R. Spikelets in Pyramidal Neurons: Action Potentials Initiated in the Axon Initial Segment That Do Not Activate the Soma. PLOS Computational Biology. 2017; 13(1): e1005237. https://doi.org/10.1371/journal.pcbi.1005237 PMID: 28068338

37. Michalikova M, Remme MWH, Schmitz D, Schreiber S, Kempter R. Spikelets in pyramidal neurons: generating mechanisms, distinguishing properties, and functional implications. Reviews in the Neurosciences. 2020; 31(1):101–119. https://doi.org/10.1515/revneuro-2019-0044

38. Hu W, Shu Y. Axonal bleb recording. Neurosci Bull. 2012; 28(4):342–350. https://doi.org/10.1007/s12264-012-1247-1 PMID: 22833034

39. Almog M, Korngreen A. Is realistic neuronal modeling realistic? Journal of Neurophysiology. 2016; 116 (5):2180–2209. https://doi.org/10.1152/jn.00360.2016 PMID: 27535372

40. Hodgkin AL, Huxley AF. A quantitative description of membrane current and its application to conduction and excitation in nerve. The Journal of Physiology. 1952; 117(4):500–544. https://doi.org/10.1113/jphysiol.1952.sp004764 PMID: 12991237

41. Yin L, Rasch MJ, He Q, Wu S, Dou F, Shu Y. Selective Modulation of Axonal Sodium Channel Subtypes by 5-HT $_{1A}$ Receptor in Cortical Pyramidal Neuron. Cereb Cortex. 2015; p. bhv245. https://doi.org/10.1093/cercor/bhv245

42. Boucher PA, Joós B, Morris CE. Coupled left-shift of Nav channels: modeling the Na+-loading and dysfunctional excitability of damaged axons. J Comput Neurosci. 2012; 33(2):301–319. https://doi.org/10.1007/s10827-012-0415-7 PMID: 22476614

43. Joos B, Barlow BM, Morris CE. Calculating the Consequences of Left-Shifted Nav Channel Activity in Sick Excitable Cells. In: Chahine M, editor. Voltage-gated Sodium Channels: Structure, Function and Channelopathies. vol. 246. Cham: Springer International Publishing; 2017. p. 401–422. https://doi.org/10.1007/164_2017_63

44. Ma Y, Huguenard JR. Reemerging role of cable properties in action potential initiation. PNAS. 2013; 110(10):3715–3716. https://doi.org/10.1073/pnas.1300520110 PMID: 23440200

45. Filipis L, Canepari M. Optical measurement of physiological sodium currents in the axon initial segment. J Physiol. 2021; 599(1):49–66. https://doi.org/10.1113/JP280554 PMID: 33094478

46. Zhu JJ. Maturation of layer 5 neocortical pyramidal neurons: amplifying salient layer 1 and layer 4 inputs by Ca2+ action potentials in adult rat tuft dendrites. The Journal of Physiology. 2000; 526(3):571–587. https://doi.org/10.1111/j.1469-7793.2000.00571.x PMID: 10922009

47. Carnevale NT, Hines ML. The NEURON book. Cambridge, UK; New York: Cambridge University Press; 2006.

48. McDougal RA, Hines ML, Lytton WW. Reaction-diffusion in the NEURON simulator. Front Neuroinform. 2013; 7. https://doi.org/10.3389/fninf.2013.00028 PMID: 24298253

49. Samson E, Marchand J, Snyder KA. Calculation of ionic diffusion coefficients on the basis of migration test results. Mat Struct. 2003; 36(3):156–165. https://doi.org/10.1617/14002